Phytochemistry 187 (2021) 112747

Contents lists available at ScienceDirect

Phytochemistry

journal homepage: www.elsevier.com/locate/phytochem

Metabolite profiling reveals a role for intercellular dihydrocamalexic acid in the response of mature *Arabidopsis thaliana* to *Pseudomonas syringae*

Christine J. Kempthorne [a,b,c,*], Alexander J. Nielsen [b], Daniel C. Wilson [b], James McNulty [b], Robin K. Cameron [b], David K. Liscombe [a,c,1]

[a] Vineland Research and Innovation Centre, 4890 Victoria Ave North Box 4000, Vineland Station, Ontario, L0R 2E0, Canada
[b] McMaster University, 1280 Main St W, Hamilton, Ontario, L8S 4L8, Canada
[c] Brock University, 1812 Sir Isaac Brock Way, St Catharines, Ontario, L2S 3A1, Canada

ARTICLE INFO

Keywords:
Arabidopsis thaliana (L.) heynh
Brassicaceae
Age-related resistance
Intercellular space
Metabolomics
Antimicrobial
Indolic
Cytochrome P450
Dihydrocamalexic acid

ABSTRACT

The leaf intercellular space is a site of plant-microbe interactions where pathogenic bacteria such as *Pseudomonas syringae* grow. In *Arabidopsis thaliana,* the biosynthesis of tryptophan-derived indolic metabolites is induced by *P. syringae* infection. Using high-resolution mass spectrometry-based profiling and biosynthetic mutants, we investigated the role of indolic compounds and other small molecules in the response of mature *Arabidopsis* to *P. syringae*. We observed dihydrocamalexic acid (DHCA), the precursor to the defense-related compound camalexin, accumulating in intercellular washing fluids (IWFs) without further conversion to camalexin. The indolic biosynthesis mutant *cyp71a12/cyp71a13* was more susceptible to *P. syringae* compared to mature wild-type plants displaying age-related resistance (ARR). DHCA and structural analogs inhibit *P. syringae* growth (MIC ~ 500 μg/mL), but not at concentrations found in IWFs, and DHCA did not inhibit biofilm formation *in vitro*. However, infiltration of exogenous DHCA enhanced resistance in mature *cyp71a12/cyp71a13*. These results provide evidence that DHCA derived from CYP71A12 and CYP71A13 activity accumulates in the intercellular space and contributes to the resistance of mature *Arabidopsis* to *P. syringae* without directly inhibiting bacterial growth.

1. Introduction

The leaf intercellular space comprises the air-filled area between plant cells (including the cell wall) and fluids that accumulate along the plant cell wall (O'Leary et al., 2014). This dynamic environment is the site of beneficial and pathogenic plant-bacteria interactions; within hours of pathogen detection, conditions in the intercellular space change in an attempt to prevent bacterial colonization (Delaunois et al., 2014; Naseem et al., 2017; O'Leary et al., 2016). Intercellular components can be studied by infiltrating the leaf intercellular space with water, solvents, or buffers, followed by collecting the intercellular washing fluids through centrifugation. Intercellular washing fluids (IWFs) contain plant and bacterial metabolites and components from the plant cell wall (O'Leary et al, 2014, 2016; Soylu et al., 2005). Specialised metabolites with antimicrobial activity (also known as phytoalexins) accumulate in response to pathogen exposure (Darvill and Albersheim, 1984; Pedras et al., 2011) and localization of specialised metabolites to the intercellular space may act to limit the pathogenicity of bacteria, but the identity of these compounds and their mode(s) of action are not well understood (Agrawal et al., 2010; Forcat et al., 2010; O'Leary et al, 2014, 2016; Soylu et al., 2005; Wilson et al., 2017).

Age is a relevant factor in the outcome of plant-pathogen and plant-herbivore interactions, as many plants become more resistant to pathogens and pests as they mature (Develey-Rivière and Galiana, 2007; Whalen, 2005). In the model species *Arabidopsis thaliana*, resistance to *Pseudomonas syringae*, *Hyaloperonospora arabidopsis* (downy mildew), and the herbivore *Trichoplusia ni* (cabbage looper larvae) increases with age (Carviel et al., 2014; Kus et al., 2002; Rusterucci et al., 2005; Tucker and Avila-Sakar, 2010). In several cases, age-related resistance (ARR) has been associated with changes in specialised metabolite

* Corresponding author. Vineland Research and Innovation Centre, 4890 Victoria Ave North Box 4000, Vineland Station, Ontario, L0R 2E0, Canada.
E-mail addresses: christine.kempthorne@vinelandresearch.com (C.J. Kempthorne), david.liscombe@vinelandresearch.com (D.K. Liscombe).

[1] This work was completed at the Vineland Research and Innovation Centre, 4890 Victoria Ave North Box 4000, Vineland Station, Ontario, L0R 2E0, Canada; the Centre for Microbial Chemical Biology, 1200 Main St W MDCL-2330, Hamilton, Ontario, L8S 4K1, Canada; and the Departments of Biology and Chemistry and Chemical Biology, McMaster University, 1280 Main St W, Hamilton, Ontario, L8S 4L8, Canada.

https://doi.org/10.1016/j.phytochem.2021.112747
Received 8 December 2020; Received in revised form 14 March 2021; Accepted 18 March 2021
Available online 3 April 2021

accumulation. For example, Mansfeld et al. (2017) used non-targeted metabolomics to show that terpenoids and flavonoids in mature fruit peels are a major contributor to cucumber fruit resistance against the oomycete *Phytophthora capsici*. Similarly, *Datura* species produce tropane alkaloids as they age, which are thought to contribute to developmental resistance against herbivores (Kariñho-Betancourt et al., 2015). In *A. thaliana*, intercellular washing fluids from mature ARR-responding plants exhibit antimicrobial activity against *P. syringae* pathovar tomato *(Pst) in vitro,* and intercellular accumulation of salicylic acid (SA) plays a role in inhibition of growth and biofilm formation of *Pst* (Cameron and Zaton, 2004; Kus et al., 2002; Wilson et al., 2017). Biofilms are composed of bacterial cell aggregates embedded in a matrix of polysaccharides, extracellular DNA, and proteins that provide a protective environment against antimicrobials (Costerton et al., 1999; Donlan and Costerton, 2002). The formation of biofilm involves bacteria sensing and responding to environmental cues, and bacteria in biofilms have different metabolic and gene expression profiles than free-swimming planktonic bacteria, which can contribute to antibiotic resistance or susceptibility (de Kievit et al., 1999; Masák et al., 2014). Inhibition of virulence factors involved in biofilm formation but not growth may be a successful strategy for plants since it reduces selection for antibiotic-resistant populations (Lee et al., 2012; Lewis and Ausubel, 2006). Biofilm-like aggregation has been reported for *P. syringae* pv. *Actinidiae* and pv. *Phaseolicola* in the intercellular space of kiwifruit and

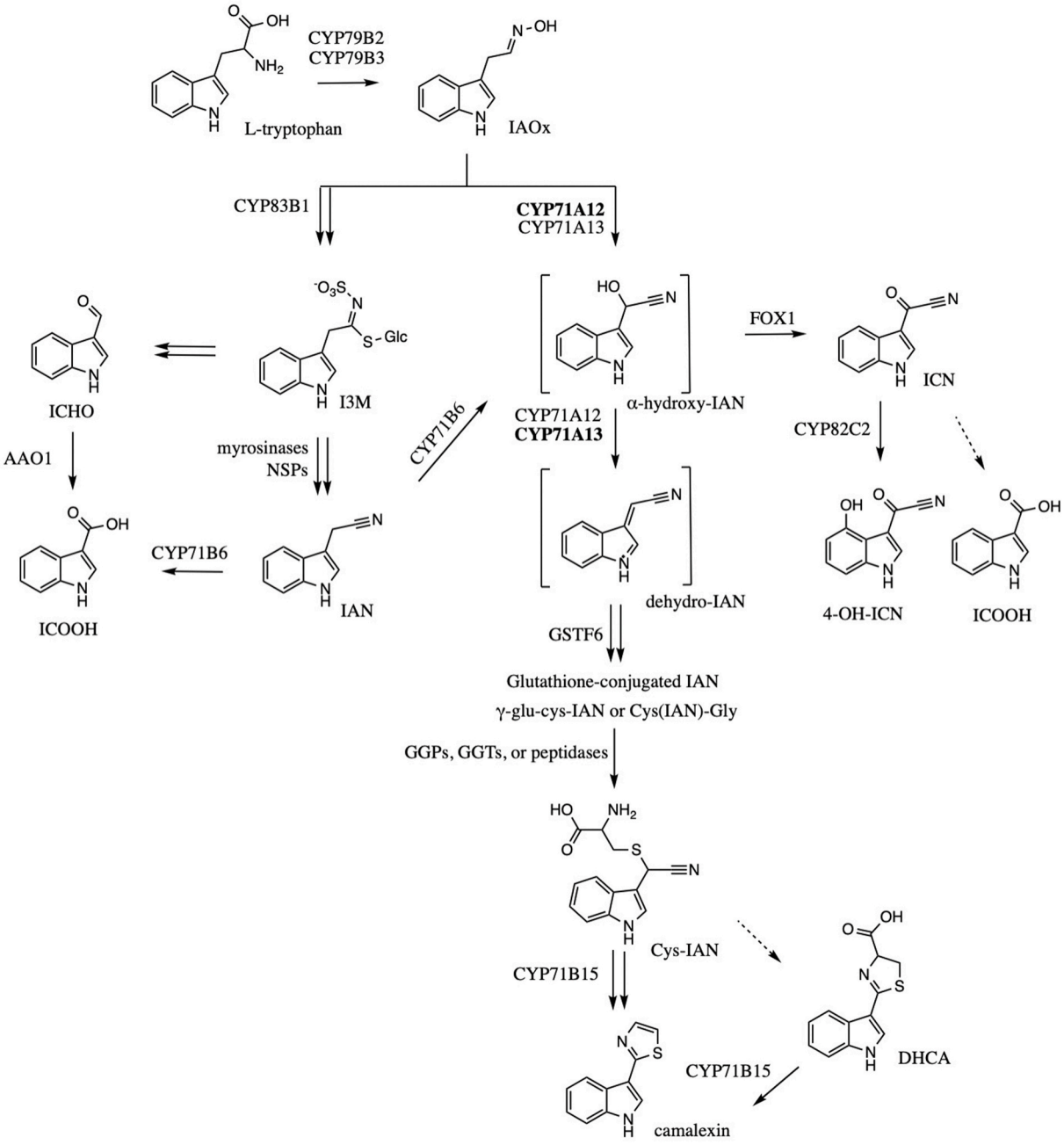

Fig. 1. Biosynthesis pathway of tryptophan-derived specialised metabolism in *Arabidopsis thaliana* (simplified). Dashed arrows indicate potential non-enzymatic reactions. Multiple arrows indicate multiple reaction steps simplified for presentation. IAOx: indole-3-acetaldoxime, I3M: indole-3-methylglucosinolate, IAN: indole-3-acetonitrile, ICHO: indole-3-carbaldehyde, ICOOH: indole-3-carboxylic acid, ICN: indole-3-carbonyl nitrile, 4-OH-ICN: 4-hydroxyindole-3-carbonyl nitrile, NSP: nitrile-specifier protein, FOX1: flavin-dependent oxidoreductase, AAO1: Arabidopsis aldehyde oxidase I, GGP: gamma-glutamyl peptidase, GGT: gamma-glutamyl transpeptidase DHCA: dihydrocamalexic acid. Modified from Rajniak et al. (2015); Müller et al. (2019).

beans respectively (Ghods et al., 2015; Manoharan et al., 2015) and for *Pst* in the intercellular space of *A. thaliana* leaves using GFP-expressing bacteria (Wilson et al., 2017). In Arabidopsis, accumulation of tryptophan (trp)-derived indolic metabolites has been observed in response to *P. syringae* (Forcat et al., 2010; Glazebrook and Ausubel, 1994; Rajniak et al., 2015; Zhou et al., 1999).

Biosynthesis of indolic metabolites in Arabidopsis leaves begins with CYP79B2 and CYP79B3 producing indole-3-acetaldoxime (IAOx), followed by CYP71A12-and CYP71A13-mediated conversion of IAOx to two reactive indole-3-acetonitrile (IAN) intermediates, alpha-hydroxy IAN and dehydro-IAN (Nafisi et al., 2007; Zhao, 2002, Fig. 1). *CYP71A12* and *CYP71A13* form a metabolic branchpoint in the biosynthesis of three main classes of defense-related indole molecules: indole-3-carboxylic acid (ICOOH) derivatives, indole carbonylnitrile (ICN) derivatives, and camalexin (Böttcher et al., 2009; Klein et al., 2013; Møldrup et al., 2013a; Müller et al., 2019, 2015; Nafisi et al., 2007; Rajniak et al., 2015, Fig. 1). In the case of camalexin biosynthesis, alpha-hydroxy IAN is converted to dehydro-IAN mainly through CYP71A13 activity with minor contribution from CYP71A12 activity (Klein et al., 2013; Rajniak et al., 2015). Dehydro-IAN is conjugated to glutathione (GSH(IAN)) and catabolized to a cysteine conjugated form (Cys (IAN)) through γ-glutamyl peptidase and/or γ-glutamyl transpeptidase activity (Geu-Flores et al., 2011; Møldrup et al., 2013b; Su et al., 2011). Cys (IAN) cyclizes non-enzymatically to form dihydrocamalexic acid (DHCA) and is also the substrate for the multifunctional enzyme CYP71B15, which catalyzes the formation of both DHCA and camalexin through two sequential reaction steps (Böttcher et al., 2009; Schuhegger et al., 2006; Zhou et al., 1999, Fig. 1).

Alpha-hydroxy-IAN is converted to ICN via FOX1 activity or to indole-3-carbaldehyde and indole-3-carboxylic acid via CYP71B6 and AAO1 activity (Böttcher et al., 2009; Rajniak et al., 2015). CYP71A12 activity, but not CYP71A13, is responsible for ICN biosynthesis, and ICOOH biosynthesis in response to pathogens (Rajniak et al., 2015; Pastorczyk et al., 2020). The expression of *CYP71A13* was previously reported as upregulated in mature wild type (Col-0) *A. thaliana* in response to *Pst* at 12 h post-inoculation (Carviel et al., 2014). The flux of CYP71A12 and CYP71A13 intermediates is affected by the type of stressor plants are exposed to for induction of the pathway; CYP71A12-mediated ICOOH biosynthesis in response to abiotic stressors like UV exposure can be partially compensated for by CYP71A13 (Müller et al., 2015), but in response to fungal pathogens such as *Plectosphaerella cucumerina* CYP71A12 is required for accumulation of ICOOH derivatives independent of CYP71A13 activity (Pastorczyk et al., 2020).

In this work, we sought to investigate the potential role of intercellular indolic compounds involved in mature *A. thaliana* at 7 weeks post-germination (vegetative phase). We screened the resistance phenotypes of *cyp71a13* and *cyp71a12/cyp71a13* mutants to *Pst* and used a non-targeted, high-resolution mass spectrometry-based approach to analyze IWFs collected from resistant and susceptible genotypes to identify indolic derivatives and other small molecules that become localized to the intercellular space of leaves in response to *Pst.* The identification of DHCA without further conversion to camalexin in IWFs from mature *Pst*-infiltrated leaves led us to examine this compound's role in *A. thaliana's* bacterial defense through growth inhibition, biofilm inhibition, and *in planta* resistance assays.

2. Results and discussion

2.1. Susceptibility of indolic biosynthesis mutants to P. syringae

CYP71A12, *CYP71A13,* and *CYP71B15* transcripts are upregulated in response to a broad range of biotic and abiotic stressors, including heavy metal salts, reactive oxygen species, UV irradiation, mechanical wounding, fungal interaction, and *P. syringae* (Frerigmann et al., 2015; Glawischnig et al., 2004; Müller et al., 2019; Nafisi et al., 2006; Pastorczyk et al., 2020; Zhou et al., 1999). To examine the role of CYP71A13 in the response of mature *A. thaliana* to *Pst* we initially screened the *cyp71a13* TDNA insertion mutant for ARR defects. The *cyp71a13* mutant had an inconsistent ARR response; it supported wild-type levels of bacteria at 3 weeks old (Table S1.1), but at 7 weeks old had a variable response to *Pst*, supporting wild-type levels of bacteria in six of seven experiments (Table S1.2). The amino acid sequence of CYP71A12 is 89% identical to CYP71A13 and can partially compensate for the loss of *CYP71A13* as demonstrated using *in vitro* and heterologous pathway reconstitution and metabolite profiling of biosynthetic mutants (Böttcher et al., 2009; Klein et al., 2013; Morten E. Møldrup et al., 2013b; Müller et al., 2015; Nafisi et al., 2007; Pastorczyk et al., 2020), which may explain the variable response to *Pst* of mature *cyp71a13*. The partial redundancy of CYP71A12 and CYP71A13 and the tandem location of these genes made it difficult to study the role of this pathway in resistance until Müller et al. (2015) developed a *cyp71a12/cyp71a13* double mutant through gene editing. The mature *cyp71a12/cyp71a13* double mutant is consistently more susceptible to *Pst*, supporting 2- to 8-fold higher bacterial levels compared to mature Col-0 (Fig. 2, Table S1.2).

CYP71B15 acts downstream of CYP71A12 and CYP71A13 in the biosynthesis of camalexin and the *cyp71b15* mutant displayed a wild-type ARR response to *Pst* inoculation by pressure infiltration into the intercellular space regardless of age (Fig. 2, Table S1.1, S1.2). Previous studies using pressure infiltration for inoculation have also reported that *CYP71B15* is not required for resistance to *P. syringae* (Glazebrook and Ausubel, 1994). Rajniak et al. (2015) showed that *cyp71b15* (4–5 weeks post-germination) was more susceptible to *Pst* than Col-0 when using a spray-inoculation technique meant to represent the natural infection process more accurately, whereby bacteria on the leaf surface can only enter the intercellular space via stomatal openings. Since we were searching for potential intercellular antimicrobial compounds, we pressure infiltrated bacteria directly into the intercellular space of leaves to bypass the potential confounding effects of disruption of stomatal signaling mechanisms that have been shown to occur in some mutants for biosynthetic genes (Baccelli et al., 2014; Melotto et al., 2006). The

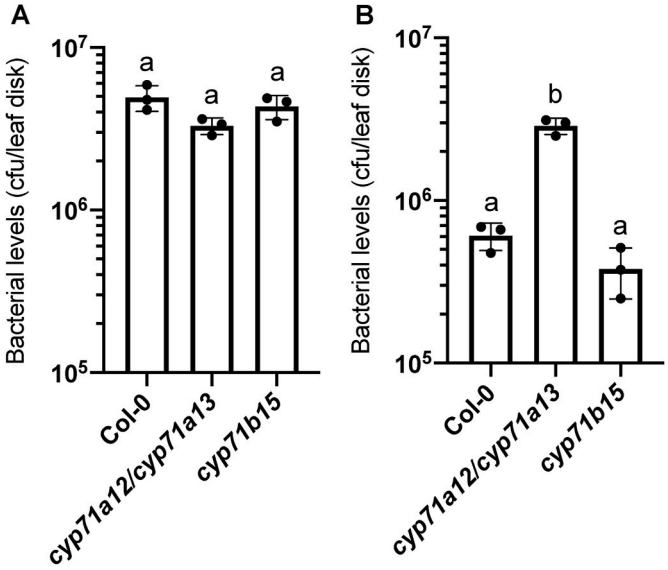

Fig. 2. The *cyp71a12/cyp71a13* mutant supports higher levels of *Pseudomonas syringae* at 7 weeks post-germination compared to Col-0 and *cyp71b15*. *P. syringae* pv. Tomato levels were quantified 3 days after inoculation by pressure infiltration of fully expanded rosette leaves of (A) 3- or (B) 7-week-old plants. Values represent the mean ± standard deviation of three sample replicates ($n = 3$) consisting of 8 plants each. Different letters indicate statistically significant differences (one-way ANOVA, Tukey's honestly significant difference [HSD], $P < 0.05$).

cyp71a12/cyp71a13 and *cyp71b15* mutants both produce trace amounts of camalexin (Böttcher et al., 2009; Müller et al., 2015; Zhou et al., 1999) yet differed in their resistance phenotypes, which indicated camalexin is not contributing to *Pst* resistance in mature *A. thaliana* as an antimicrobial and suggested a possible role for other trp-derived metabolites produced as a result of CYP71A13 and/or CYP71A12 activity.

2.1.1. Non-targeted metabolite profiling of intercellular washing fluids in response to P. syringae

As mentioned, CYP71A12 and CYP71A13 form a metabolic branch point in the production of precursors that serve as a substrate for enzymes in trp-derived specialised metabolism, so it was unknown which, if any, downstream compounds were present in the intercellular space in response to *Pst*. Therefore, we used non-targeted, high-resolution mass spectrometry-based metabolomics to examine the accumulation of all detectable semi-polar metabolites in mature plants' intercellular space after *Pst* inoculation in Col-0, *cyp71b15* (wild-type resistance despite perturbation in trp-derived metabolite pathway downstream of CYP71A12 and CYP71A13), and *cyp71a12/cyp71a13* (increased susceptibility to *Pst* when mature compared to Col-0). We focused on mature plants because of the increased susceptibility observed in mature *cyp71a12/cyp71a13* in ARR assays and because 7-week-old rosette leaves were well suited for the infiltration-centrifugation technique (O'Leary et al., 2014) used to collect required volumes of intercellular washing fluids (IWFs) for metabolite profiling from mock- and *Pst*-inoculated plants. Minimal cytoplasmic contamination in IWFs was confirmed by assessing chlorophyll levels spectrophotometrically (Baker et al., 2012).

To identify mass spectral features that may be important for *Pst* resistance in mature plants, we first performed a pairwise comparison via volcano plot between mock- and *Pst*-inoculated wild type IWFs (Fig. S1). Principal component analysis (PCA) of all features showed that the first two components account for 93.7% of the total variance in IWFs run in positive ESI mode (Fig. S2A) and 90.4% of the total variance in negative ESI mode (Fig. S2B). Mock- and *Pst*-inoculated samples formed distinct clusters in both ESI modes, although the clusters are more separated in negative ESI mode. In total, 26 features were found to be significantly different between IWFs from wild type mock- and *Pst*-inoculated leaves (Fig. S1; Table S2.1, 2.2, 2.3). Next, we compared the accumulation of these 26 features between susceptible and resistant genotypes by including IWFs collected from *cyp71b15* (wild-type *Pst* resistance) and *cyp71a12/cyp71a13* (increased susceptibility to *Pst*) using one-way ANOVA (Fig. S3). We pursued mass features that could be functional in resistance to *Pst*, rather than features solely reflecting perturbation of trp-derived specialised metabolism in *cyp71a12/cyp71a13*. These compounds should have different accumulation patterns in the resistant genotypes (Col-0 and *cyp71b15*) compared to susceptible ones (*cyp71a12/cyp71a13*). Two features were significantly different between resistant (Col-0, *cyp71b15*) and susceptible (*cyp71a12/cyp71a13*) genotypes (Fig. S3-E, Q): one at 6.96 min with a nominal mass of *m/z* 322 corresponding to a glycosylated indole-3-carboxylic acid (ICOOH), and the other at 7.32 min with a nominal mass of *m/z* 247 corresponding to the camalexin precursor, dihydroxycamalexic acid (DHCA).

The feature that eluted at 6.96 min with a nominal mass of *m/z* 322 was putatively identified as an indole-3-carboxylic acid beta-D-glucopyranosyl ester with a mass error of −1.9 ppm (*m/z* 322.0921 [$C_{15}H_{17}NO_7$–H]). Fragmentation produced peaks at *m/z* 160.0392 corresponding to an indole-3-carboxylic acid aglycone ([$C_9H_7NO_2$–H]) and *m/z* 116.0503 corresponding to an indole ring ([C_8H_7N–H]) (Fig. S4), which is consistent with fragmentation behavior for this compound noted by Böttcher et al. (2014, 2009). This feature was elevated in IWFs from resistant plants (Col-0 and *cyp71b15*) compared to IWFs from susceptible *cyp71a12/cyp71a13* plants (Fig. S3-Q). Müller et al. (2015) showed that 6-week-old *cyp71a12/cyp71a13* produces reduced levels of glycosylated ICOOH compared to wild-type Arabidopsis in response to abiotic stressors (UV exposure and silver nitrate). ICOOH derivatives are also constitutively produced but accumulate at elevated levels after pathogen challenge in Arabidopsis (Bednarek et al., 2005; Hagemeier et al., 2001; Iven et al., 2012; Pastorczyk et al., 2020). ICOOH is esterified to the cell wall in response to *P. syringae* and has been hypothesized to prevent localized bacterial aggregation or act as an antimicrobial compound by intercalating into the bacterial membrane (Forcat et al., 2010; Soylu et al., 2005). Indole-3-carboxylic acid beta-D-glucopyranosyl ester accumulated at 400–600 pmol in leaves of 6-week-old Arabidopsis in response to *Pst* at 48 h post-inoculation and was hypothesized to function as a transport intermediate for ICOOH cell wall conjugation (Hagemeier et al., 2001). Recent work by Pastorczyk et al. (2020) confirmed that CYP71A12, but not CYP71A13, is required for accumulation of two glycosylated ICOOH products (6-O-glucoside of 6-hydroxy-indole-3-carboxylic acid and indole-3-carboxylic acid glucose ester) in the leaves of 4-week-old plants in response to the fungal pathogen *Plectosphaerella cucumerina*.

It is also possible that the peak corresponding to an ICOOH glucopyranosyl ester is a degradation product of compounds derived from indole carbonylnitriles (ICNs). ICN compounds are unstable and rapidly degrade to ICOOH in aqueous solution (Rajniak et al., 2015). In the context of our work, ICN degradation to ICOOH could occur between the time bacteria (in aqueous solution) are first pressure infiltrated into the leaf intercellular space and when IWFs are collected by centrifugation 24 h later, although given the role of CYP71A12 in ICN biosynthesis (Fig. 1), we would expect a mass feature corresponding to glycosylated ICOOH to be absent from *cyp71a12/cyp71a13* if it was an ICN degradation product.

Probing the contribution of ICOOH pathways in response to bacteria in the intercellular space requires consideration of differences in constitutive and induced ICOOH pathways, the complexity of downstream derivatives (e.g., glycosylated and amino acid conjugates, indole-ring hydroxylations), and the fact that not all the genes involved in these pathways have been fully elucidated (Böttcher et al., 2014; Müller et al., 2019; Pastorczyk et al., 2020; Tan et al., 2004). Further work examining the resistance phenotype of *cyp71a12* mutants in combination with other genes with minor contribution to pathogen induced ICOOH biosynthesis (i.e., *cyp71b6, aao1*) to *Pst* may reveal more about the role of ICOOH compounds in disease resistance (Müller et al., 2019; Pastorczyk et al., 2020). Given the previously mentioned studies supporting a role for ICOOH derivatives in pathogen resistance, we chose to pursue investigation of the mass feature at 7.32 min that resembled DHCA.

2.1.2. Dihydrocamalexic acid accumulates in the intercellular space in response to P.syringae

The mass spectral feature that eluted at 7.32 min with a nominal mass of *m/z* 247 was of interest since it was only detected in IWFs collected from mature resistant genotypes inoculated with *Pst* and was not detected in mock-inoculated wild type plants and *cyp71a12/cyp71a13* regardless of treatment. This suggested that this compound could be involved in defense against *Pst* and that it is not likely to be of bacterial origin (Fig. S3-E). Based on the retention time and fragmentation pattern of two independently synthesized standards, this feature was confirmed to be the camalexin precursor, *(S)*-dihydrocamalexic acid (DHCA; *m/z* 247.0541 [$C_{12}H_{10}N_2O_2S$ + H]), with fragmentation producing peaks at *m/z* 201.0520 ([$C_{11}H_8N_2S$ + H], loss of carboxylic acid), and *m/z* 143.0604 ([$C_9H_7N_2$+H], thiazole ring-opening or fragmentation) (Böttcher et al., 2009; Zandalinas et al., 2012, Fig. 3). At 24 hpi with *Pst*, DHCA accumulated to ~0.3 μg/mL and ~0.24 μg/mL in IWFs collected from mature wild-type and *cyp71b15* plants, respectively (Fig. 4). Mock-inoculated wild-type plants did not produce detectable levels of intercellular DHCA, and mock-inoculated *cyp71b15* accumulated DHCA (~0.09 μg/mL), likely due to a block in camalexin biosynthesis whereby a cysteine-conjugated indole-3-acetonitrile (Cys (IAN)) precursor accumulates, and non-enzymatically cyclizes to produce DHCA (Böttcher et al., 2009). DHCA is not readily degraded to other

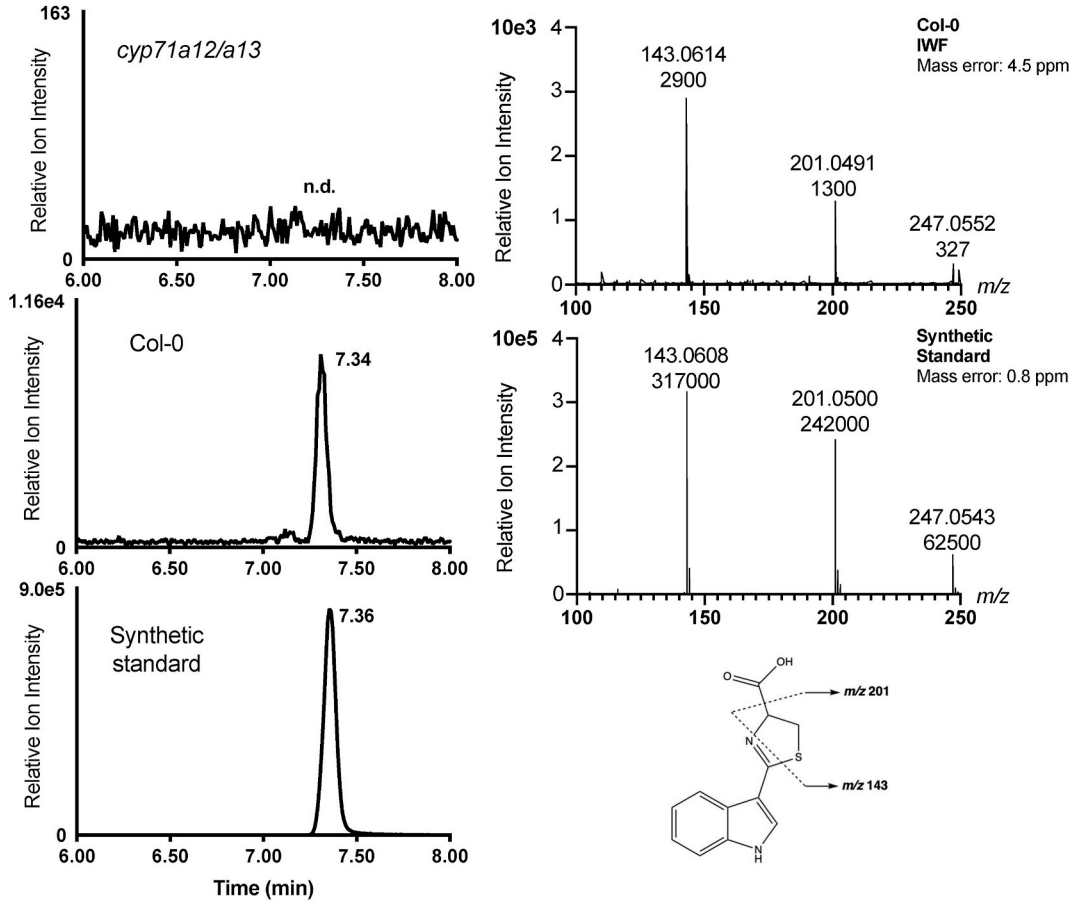

Fig. 3. Identification of dihydrocamalexic acid (DHCA) in intercellular washing fluids. Extracted ion chromatograms and mass spectra for DHCA (*m/z* 247.0541, [$C_{12}H_{10}N_2O_2S$ + H] in intercellular washing fluids from *Pseudomonas syringae*-inoculated leaves compared to a synthetic standard. (A) Extracted ion chromatograms and (B) MSMS (25 eV). n. d. Indicates compound not detected. Samples were run in positive electrospray ionization mode.

products (Böttcher et al., 2009), so in the absence of CYP71B15 in a localized area like the intercellular space, it could accumulate without being converted to camalexin. Bednarek et al. (2005) observed both DHCA and camalexin as root exudates from 4-week-old *Arabidopsis thaliana* grown in liquid culture after infection with the oomycete *Pythium sylvacticum*. Camalexin was not detected in the intercellular space, regardless of treatment or genotype (Table S3).

DHCA derivatives (DHCA methyl ester [$C_{13}H_{12}N_2O_2S$], glutathione-conjugated DHCA [$C_{17}H_{18}N_4O_4S$], and glycosylated DHCA [$C_{17}H_{17}N_3O_5S$]) that accumulate in response to silver nitrate treatment (Böttcher et al., 2009) were not detected in IWFs from mock- or *Pst*-inoculated leaves, but this does not rule out the possibility that DHCA metabolites are transported to the intercellular space where the activity of an as-yet-unidentified apoplastic process could then form DHCA. DHCA may be directly transported to the intercellular space, but the release of DHCA from CYP71B15 would have to occur during the sequential conversion of Cys (IAN) to DHCA and then camalexin (Schuhegger et al., 2006). Recent research by Mucha and colleagues (Mucha et al., 2019) suggest that metabolons consisting of CYP71A12, CYP71A13, and CYP71B15 provide efficient channeling of bioactive indolic intermediates to form camalexin; it is therefore unlikely that appreciable levels of DHCA and other intermediates are released from these enzyme complexes during camalexin biosynthesis.

Glutathione-conjugated IAN (GSH(IAN)), Cys (IAN), or intermediates formed during catabolism of GSH(IAN) to Cys (IAN) may be transported to the intercellular space where they could be converted enzymatically or non-enzymatically to DHCA. This part of the camalexin pathway is difficult to elucidate due to functional redundancy in enzyme families and *in vitro* substrate promiscuity of the enzymes hypothesized to produce these intermediates (Geu-Flores et al., 2011; Klein et al., 2013; Møldrup et al., 2013a, 2013b). In cytosolic camalexin biosynthesis, γ-glutamyl peptidase 1 (GGP1) and 3 (GGP3) are the enzymes involved in the catabolism of GSH(IAN) to Cys (IAN), and double mutants for these genes have reduced camalexin production in response to chemical inducers (Geu-Flores et al., 2011). The γ-glutamyl transpeptidases GGT1 and GGT2 are not likely to be involved in cytosolic camalexin production as *GGT1* is not upregulated in response to chemical inducers and *GGT2* is not expressed in leaves (Destro et al., 2011; Martin et al., 2007). However, given that GGT1 and GGT2 are localized to the apoplast, they could be involved in the production of DHCA in the intercellular space in response to *Pst* (Martin et al., 2007; Ohkama-Ohtsu et al., 2007). In that case, GGT1 and GGT2 involvement in DHCA biosynthesis would require transport of a glutathione-IAN conjugate such as γ-GSH-, Gly-Cys-, or Cys-Glu-(IAN) to the intercellular space.

Mucha et al. (2019) revealed a possible mechanism for how bioactive intermediates can be released during camalexin biosynthesis. They showed that glutathione-S-transferase (GST) U4 physically interacts with CYP71A13 and negatively regulates camalexin biosynthesis in response to pathogens. The regulatory mechanism is unknown, but the authors discussed the possibility that GSTs interact with an ER-associated camalexin biosynthetic metabolon to transport intermediates to other subcellular compartments. In the context of our work, intercellular DHCA may be accumulating as a result of transport of IAN conjugates from the camalexin biosynthetic metabolon, followed by cytosolic and/or intercellular GGP/GGT activity and non-enzymatic cyclization resulting in accumulation of DHCA without further conversion to camalexin by CYP71B15. This model for DHCA accumulation in

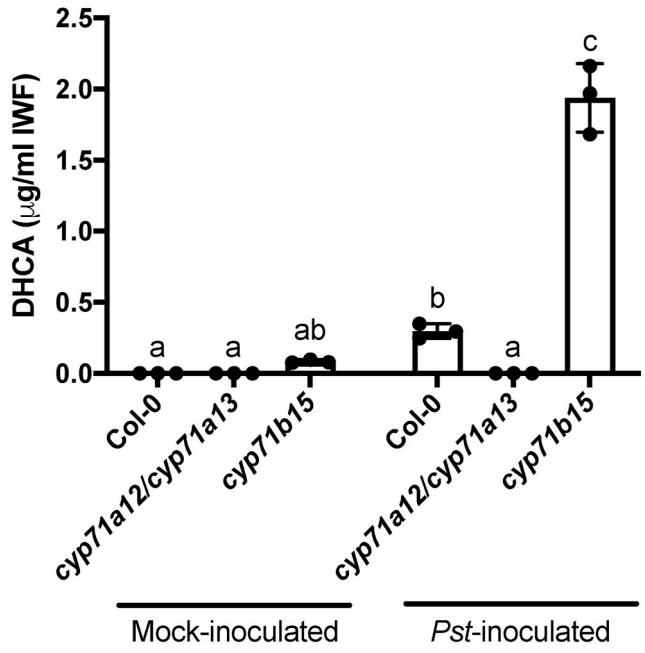

Fig. 4. Quantification of dihydrocamalexic acid (DHCA) (*m/z* 247.0541, $[C_{12}H_{10}N_2O_2S + H]$) in intercellular washing fluids (IWFs). DHCA levels measured in IWFs from Col-0, *cyp71a12/cyp71a13,* and *cyp71b15* (all 7-weeks post-germination) 24 h after inoculation with *P. syringae* (*Pst*) or 10 mM $MgCl_2$ (mock-inoculation) measured by UPLC-MS electrospray ionization in positive mode (ESI+). Values represent the mean ± standard deviation of three sample replicates ($n = 3$). Different letters indicate statistically significant differences (one-way ANOVA, Tukey's honestly significant difference [HSD], $P < 0.05$). Standard curves were prepared using synthetic DHCA (2 pg–6 μg on column).

the intercellular space (Fig. S5) is speculative at this time and mass features corresponding to IAN conjugates were not detected in IWFs at 24 hpi with *Pst* regardless of genotype or treatment (Table S3). Further work analyzing IWFs and resistance phenotypes of double, triple, or quadruple *GGP* and *GGT* mutants, *GST4U* knockouts and over-expressors, as well as screening for candidate genes encoding glutathione-conjugate ABC transporters (DeRidder and Goldsbrough, 2006; Lu et al., 1997; Tommasini et al., 1998), may reveal the genes and mechanisms involved in DHCA accumulation in the intercellular space in response to bacterial induction of the camalexin pathway.

2.1.3. Bioactivity of dihydrocamalexic acid on P. syringae growth

To examine the ability of DHCA to inhibit the growth of *Pst*, bacteria were incubated with concentrations of 0.05–1000 μg/mL DHCA and bacterial growth was measured spectrophotometrically (OD_{600}). *Hrp*-inducing minimal (HIM) medium was used for all *in vitro* assays in this work to mimic the conditions of the intercellular space and induce bacterial virulence gene expression in the bacteria (Huynh et al., 1989; Kim et al., 2009; Rahme et al., 1992). To test for *Pst*'s ability to use DHCA as a nutrient source, assays with DHCA as the sole source of carbon or nitrogen and sulfur were performed using concentrations that showed little to no bacterial growth inhibition (1–32 μg/mL). *Pst* survived, but no growth was observed, indicating that *Pst* did not use DHCA as a nutrient source (Fig. S6).

DHCA displayed inhibitory activity against *Pst* at concentrations above 96 μg/mL but did not inhibit growth at the range of concentrations observed in IWFs (0.3 μg/mL to 2.4 μg/mL). DHCA had a minimum inhibitory concentration (MIC) of ~500 μg/mL and a minimum bactericidal concentration (MBC) of ~1 mg/mL (Fig. 5A). In comparison, the MIC and MBC of salicylic acid, an intercellular compound with antimicrobial activity that contributes *Pst* observed in mature plants, is approximately 250 μg/mL and 500 μg/mL, respectively (Cameron and Zaton, 2004; Wilson et al., 2017; Fig. S7). Since current intercellular profiling techniques require full hydration of the leaf for downstream profiling, IWF measurements represent the amount of compound washed out of the intercellular space and do not account for the possibility of localized concentration gradients (Gentzel et al., 2019; Wilson et al., 2017). For example, plant metabolites may accumulate at sites of bacterial aggregation or in the cell wall at high concentrations.

2.1.4. Dihydrocamalexic acid does not inhibit P. syringae biofilm formation

Indole-3-acetonitrile (~100 μg/mL) and indole-3-acetaldehyde (~100 μg/mL) have been shown to inhibit biofilm formation of the bacterial pathogens *E. coli* O157:H7 and *Pseudomonas aeruginosa*, potentially by interfering with intercellular signaling and affecting the expression of genes required for biofilm formation without affecting bacterial growth (Lee et al., 2012). To test the activity of DHCA against *Pst* biofilm formation, a spectrophotometric 96-well plate biofilm assay was used (see Materials and Methods; O'Toole, 2011). To ensure that these tests would reflect reduced biofilm formation rather than inhibition of growth, DHCA concentrations were chosen to avoid the reduction of bacterial growth (0.3–18 μg/mL). SA was used as a positive control as it has bioactivity against *P. syringae* biofilms, inhibiting their formation *in vitro* at concentrations as low as 2 μM (~270 ng/mL). As previously observed (Wilson et al., 2017), biofilm formation was reduced in the presence of 18 μg/mL SA at 48 and 72 h (Fig. 6A). However, DHCA did not significantly affect biofilm formation at any concentrations or time points tested (Fig. 6B). These results show that DHCA does not inhibit biofilm formation of *Pst in vitro*.

2.1.5. Structure-activity relationship of DHCA chirality and indole moiety

To examine how structural components of DHCA may affect its antimicrobial activity against planktonic (free individual cells not part of an aggregate) *Pst,* structure-activity studies were completed using camalexin and synthetic enantiomers of phenylalanine and tyrosine-derived analogs of DHCA (Fig. 5). Camalexin differs structurally in that it lacks chirality provided by the carboxylic acid functional group on carbon 4 of the thiazole ring of DHCA. The antimicrobial activity of camalexin was similar to that reported for DHCA; camalexin has a MIC of ~500 μg/mL when incubated with *P. syringae* pv. *Maculicola* in camalexin-spiked IWFs (Rogers et al., 1996), and a MIC of ~250 μg/mL when incubated with *Pst* in HIM medium (Fig. 5B).

To examine how the indole ring contributes to growth inhibition against *Pst*, analogs of DHCA were synthesized with the indole ring replaced with a phenyl (Compounds **1** and **2** in Fig. 5) or a phenol (Compounds **3** and **4** in Fig. 5) group. Stereochemistry had a marked effect on antimicrobial activity for the phenyl ring analogs as analog **1** lacked growth inhibitory activity against *Pst* at any of the concentrations tested (Fig. 5C). Analog **2** was more effective at inhibiting the growth of *Pst* compared to DHCA, with a similar MIC as camalexin (~250 μg/mL; Fig. 5D); however, it was less bactericidal than DHCA and camalexin, as 1 mg/mL of analog **2** was not lethal to *Pst* (Fig. S8). Replacement of the indolic ring with a phenol moiety causes loss of antimicrobial activity regardless of stereochemistry as *Pst* growth was unaffected by incubation with analogs **3** and **4** (Fig. 5E and F).

DHCA may have a similar mode of action as camalexin for *Pst* growth inhibition but is not as effective due to the carboxylic acid moiety. Camalexin rapidly disrupts membrane integrity in *P. syringae*, and due to its lipophilic nature, it does not dissociate from dying cells such that any surviving bacterial cells continue to grow (Rogers et al., 1996). The hydroxyl substitution on the ring of compounds **3** and **4** may render the molecule less lipophilic, disrupting the association of camalexin and possibly DHCA with bacterial membranes, whereas the more lipophilic phenyl ring of compounds **1** and **2** still allows for membrane association. However, compound **1** did not inhibit *Pst* growth, while compound **2** did, indicating that chirality may affect the antibacterial activity of DHCA. Indeed, chirality can result in vastly different outcomes on the target organism, including adverse toxic effects or a loss of bioactivity

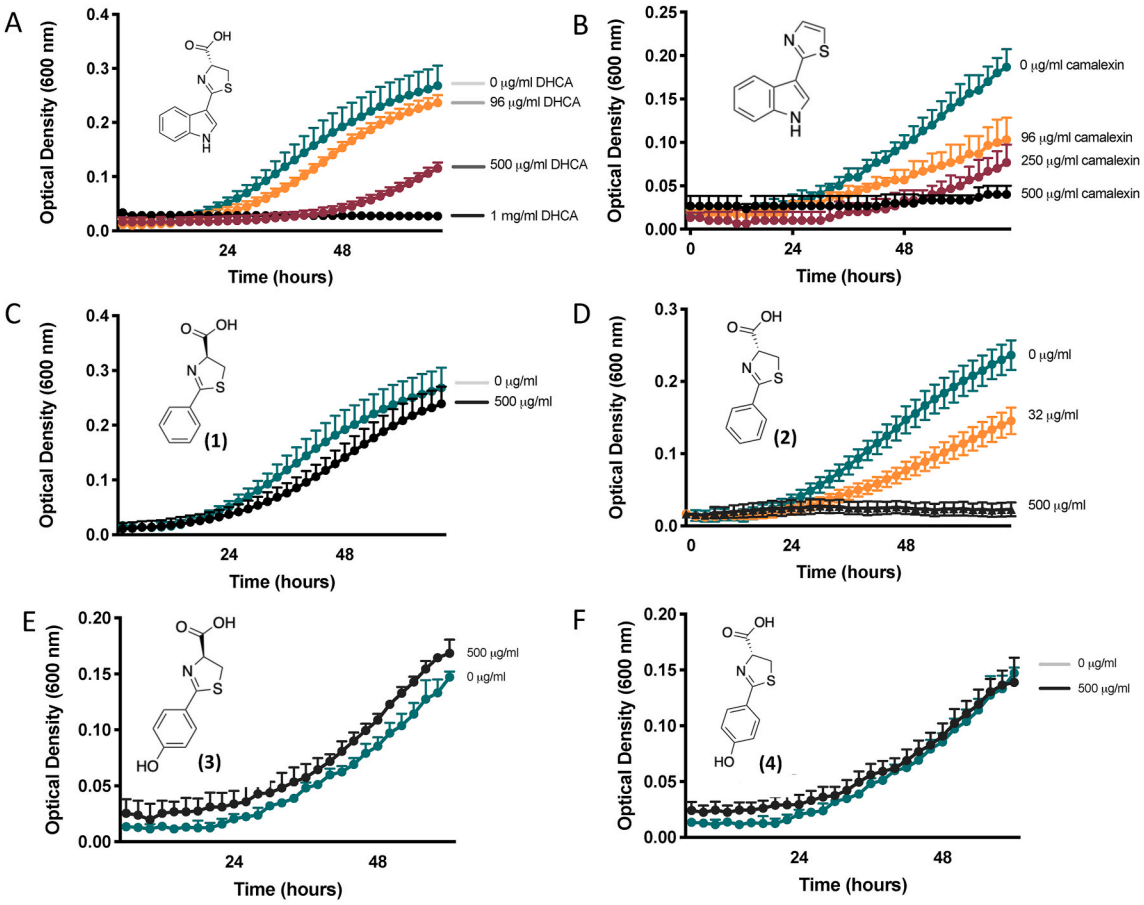

Fig. 5. Growth of *Pseudomonas syringae* (*Pst*) in the presence of dihydrocamalexic acid (DHCA), camalexin, or DHCA analogs *in vitro*. Dose-dependent effect of (*S*)-dihydrocamalexic acid (A), camalexin (B), **(1)** (*R*)-2-(phenyl)-4,5-dihydrothiazole-4-carboxylic acid (C), **(2)** (*S*)-2-(phenyl)-4,5-dihydrothiazole-4-carboxylic acid (D), **(3)** (*R*)-2-(4-hydroxyphenyl)-4,5-dihydrothiazole-4-carboxylic acid **(E)**, and (4) (*S*)-2-(4-hydroxyphenyl)-4,5-dihydrothiazole-4-carboxylic acid **(F)** on the growth of *Pst* in Hrp-inducing minimal medium as measured by turbidity (OD_{600}) after incubation for 68 h at room temperature (approximately 25 °C). Each data point is the mean ± SD of three wells per concentration from a 96-well non-tissue-culture-treated plate.

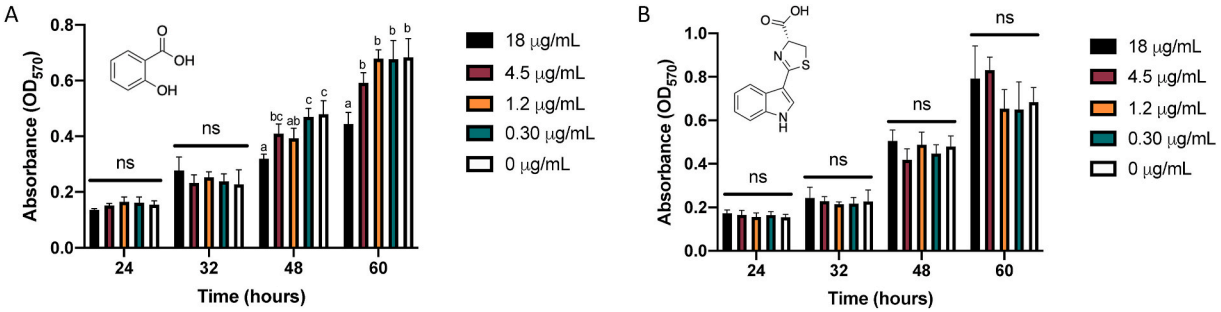

Fig. 6. Effect of dihydrocamalexic acid (DHCA) and salicylic acid (SA) on biofilm formation of *Pseudomonas syringae* (*Pst*) *in vitro*. Dose-dependent effect of (A) SA and (B) DHCA on *Pst* biofilm formation in Hrp-inducing minimal medium as measured by crystal violet staining of surface-adherent cells and de-staining with acetic acid (OD_{570}) after stationary incubation for 24, 32, 48, or 60 h. Each data point is the mean ± SD of five wells per concentration from a 96-well non-tissue-culture-treated plate. Different letters indicate statistically significant differences (one-way ANOVA, Tukey's honestly significant difference [HSD], $P < 0.05$). Ns indicates not significant. Bars (from left to right) within each timepoint are: 18 μg/mL, 4.5 μg/mL, 1.2 μg/mL, 0.3 μg/mL, and 0 μg/mL. (For interpretation of the references to color in this figure legend, the reader is referred to the Web version of this article.)

(Hutt and O'Grady, 1996; Smith, 2009). Comparing the antimicrobial activity of (S)-DHCA and (R)-DHCA could clarify whether chirality is a contributing factor to bacterial growth inhibition. To our knowledge, this is the first study examining antimicrobial activity of DHCA. Additional investigation is required to understand the bio-transformations and potential target interactions between DHCA and bacteria.

2.2. Dihydrocamalexic acid treatment restores bacterial resistance in *cyp71a12/cyp71a13*

The absence of DHCA in IWFs from *cyp71a12/cyp71a13* does not necessarily indicate a role for DHCA in resistance to *Pst*. Rather, our results may be due to the blockage of DHCA production in *cyp71a12/cyp71a13*. *In vitro* assays demonstrated that DHCA inhibited *Pst* growth at concentrations higher than those quantified in IWF samples, and

DHCA did not inhibit biofilm formation of *Pst*. However, *in vitro* antimicrobial studies do not capture the complex metabolic and physiological changes occurring in plants responding to pathogens (Bednarek and Osbourn, 2009). If DHCA is important for the response of mature plants to *Pst,* then reintroducing the compound should restore resistance to *cyp71a12/a13* plants. To test this, exogenous DHCA (0.07 μg/mL or 0.25 μg/mL) was pressure-infiltrated into the intercellular space of rosette leaves 24 h post-inoculation with *Pst*.

Infiltration of DHCA at a concentration similar to that quantified in wild type IWFs (0.25 μg/mL; 1.02 μM) 24 h after mock or *Pst* inoculation restored wild-type levels of resistance in mature *cyp71a12/cyp71a13*, causing a 10-fold reduction in bacterial levels compared to mock-inoculated plants (Fig. 7). Infiltration of a lower level of DHCA (0.07 μg/mL; 0.28 μM) resulted in a modest increased resistance in *cyp71a12/cyp71a13*, causing a 1.6-fold reduction in bacterial levels compared to mock-inoculated plants (Fig. 7). Wild-type resistance to *Pst* in mature plants was not significantly affected by infiltration of either concentration of DHCA and did not exhibit an enhanced resistance response.

Combined with our antimicrobial studies, these results suggest that DHCA affects *Pst* pathogenicity via mechanisms other than direct antimicrobial activity (e.g., by affecting enzyme activity, receptor binding, affecting plant defense or bacterial virulence signaling) or requires other compounds (e.g., ICOOH-beta-D-glucopyranosyl ester) for additive/synergistic interactions to be fully effective – mechanisms plants use to avoid the development of bacterial resistance (Bednarek and Osbourn, 2009; Khameneh et al., 2019; Lewis and Ausubel, 2006; Silva et al., 2016). *In vitro* studies have demonstrated that camalexin inhibits glycolysis, TCA pathway gene expression and reduces mycelial growth in *A. brassicicola* (Pedras et al., 2014). Camalexin has also been shown to inhibit fungal detoxification enzymes involved in the metabolism of the plant defense compounds brassinin and cyclobrassinin in isolates from canola and brown mustard (Pedras and Abdoli, 2017). Likewise, DHCA may interfere with *Pst* virulence genes or proteins through binding interactions or affecting changes in plant or bacterial gene expression. If this is the case, it would explain why the concentration of DHCA in IWFs from resistant plants does not directly inhibit bacterial growth *in vitro* and why mature *cyp71b15* does not display enhanced resistance to *Pst* despite an ~6.5-fold increase in intercellular DHCA compared to mature wild type plants.

3. Conclusion

Using a metabolomics approach with two biosynthetic mutants in the *A. thaliana* trp-derived specialised metabolism pathway, two mass spectral features (corresponding to a glycosylated indole-3-carboxylic acid derivative and dihydrocamalexic acid) were identified in intercellular washing fluids. Both compounds accumulated in response to *Pst* and to different extents in mature resistant and susceptible genotypes. We confirmed that differential accumulation had a function in plant defense since *cyp71a12/cyp71a13* was more susceptible to *Pst* and defective for intercellular DHCA accumulation. Also, exogenous infiltration of DHCA into the intercellular space at 24 hpi with *Pst* increased the resistance response of mature *cyp71a12/cyp71a13* b y reducing bacterial levels in leaves. Since DHCA does not exhibit antibiofilm activity *in vitro* and is weakly antimicrobial against *Pst* growth *in vitro* at concentrations quantified in IWFs, our results suggest that the mechanism of action for DHCA bioactivity against *Pst* is not likely through direct antimicrobial activity. Our results also suggest that DHCA, IAN-conjugates, or other precursors are transported to the intercellular space in response to bacterial invasion in *A. thaliana*. These results serve as a reminder that the localization of compounds is an important consideration in plant defense investigations. Overall, this work indicates a role for CYP71A13 and CYP71A12 in the mature *A. thaliana* response to *P. syringae* through the accumulation of intercellular indolic compounds.

4. Experimental

4.1. General experimental procedures

4.1.1. Plant growth

Arabidopsis thaliana (L.) Heynh (*Brassicaceae*) seeds were surface sterilized (70% ethanol followed by a solution of 30% bleach and 0.1% Tween 20 in sterile water), rinsed with ddH_2O, and suspended in 0.1% phytoblend. Seeds stratified for 2–3 days at 4 °C before plating on Murashige and Skoog (MS) basal salt medium (Murashige and Skoog, 1962) and germinated in under continuous light (22 °C, light intensity ~90 μmol/m^2/s, ~45% humidity). At 6–7 days, seedlings were transplanted to soil (Sunshine Mix No. 1 – JUIC Ltd.) prepared with 2 L of 1 g/L 20-20-20 fertilizer per tray. To maintain high humidity, seedlings were covered with a plastic transparent dome for 48 h in growth chambers and grown at 22 °C–24 °C at ~80% relative humidity under a 9-h photoperiod (average light intensity ~120 μmol/m^2/s). Plants were fertilized with 1 g/L of 20–20-20 fertilizer at 3 weeks post-germination (wpg) and 5 wpg. At 3- and 7-weeks post-germination (wpg), plants were used in disease resistance assays (described below). All mature plants were 7 wpg and in vegetative phase (no bolts or flowers present).

4.1.2. Plant lines

All mutant lines are *Arabidopsis thaliana* (L.) Heynh (*Brassicaceae*) in the Columbia (Col-0) accession background. The *cyp71a12* (GABI_127H03) mutant line was obtained from The Arabidopsis

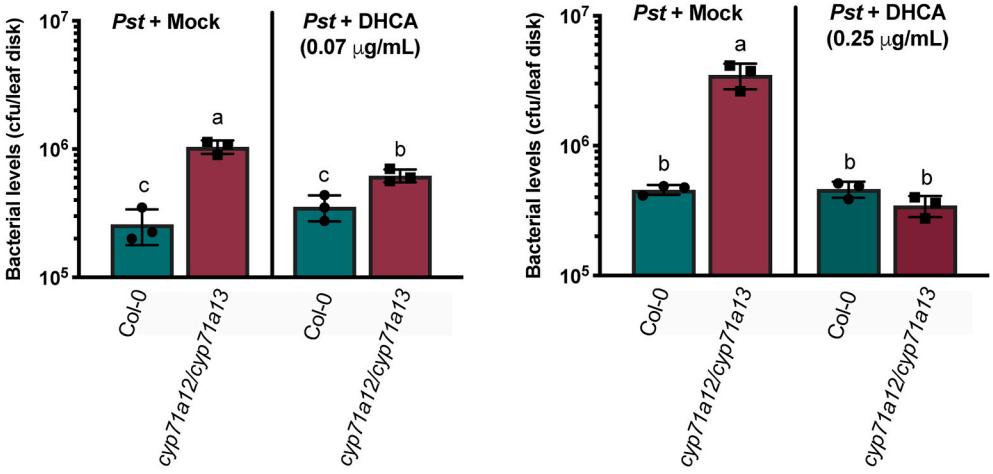

Fig. 7. Exogenous infiltration of dihydrocamalexic acid (DHCA) and bacterial quantification of *Pseudomonas syringae* in rosette leaves of 7-week old Col-0 and *cyp71a12/cyp71a13*. DHCA (0.07 μg/mL or 0.25 μg/mL) was applied via pressure infiltration to 7-week-old plants at 24 h post-inoculation with *P. syringae* or mock solution (0.06% DMSO in 10 mM $MgCl_2$). Bacterial levels were quantified at 3 days post-inoculation with *Pst*. Values represent the mean ± standard deviation of three sample replicates ($n = 3$) consisting of 8 plants each. Different letters indicate statistically significant differences (ANOVA, Tukey's honestly significant difference [HSD], $P < 0.05$).

Information Resource (TAIR). The *cyp71b15* (*pad3-1*) line was obtained from J. Glazebrook (University of Minnesota, St. Paul, MN, USA). The *cyp71a12/a13-1* line was provided by E. Glawischnig (TUM Campus Straubing for Biotechnology and Sustainability, Technical University of Munich, Germany). Individual plants homozygous for the *cyp71a13-1* T-DNA insertion were confirmed using PCR as described in Nafisi et al. (2007). Gene-specific primers designed to identify wild-type *CYP71A13*: 5′-GTAAGAGAAGACGAGGTAAATGC-3' (forward) and 5′-CTTCTGATCAGTTCCGTCATCG-3' (reverse). The primer sequence used to identify the T-DNA left border in *cyp71a13-1* was 5′-GGAACAACACTCAACCCTATCTCG-3' (LBe). The TALENs-mediated 5 base pair deletion in *CYP71A12* was confirmed via sequencing using primers 5′-TGACATTCCGCAATCTGAAAACC-3' (forward) and 5′- GGGAGAAGGATTTGTCCAGGG-3' (reverse).

4.1.3. Disease resistance assays

Virulent *P. syringae* pv. *Tomato* (*Pst*) DC3000 (pVSP61) (Whalen et al., 1991) cultures were prepared in King's B (KB) medium supplemented with 50 μg/mL kanamycin (plasmid resistance) and grown overnight with agitation at 200 rpm for ~16 h at 22–25 °C to mid-log phase (OD_{600} = 0.2 to 0.6). Cultures were re-suspended and diluted to 10^6 colony forming units (cfu) per mL of 10 mM $MgCl_2$. Medium-sized rosette leaves (fully expanded) were inoculated by pressure infiltration of dilute cultures into the abaxial (underside) surface of three leaves per plant using a needle-less 1 mL syringe. Control mock-inoculations consisted of 10 mM $MgCl_2$. Leaf disks were removed from leaves of 3- or 7-week-old plants at 3 days post-inoculation (dpi) using a cork-borer (6 mm diameter) for a total of three replicates of eight leaf disks each (one leaf disk per leaf per plant) sampled from 24 plants per treatment. *Pst* was isolated from tissue by submerging leaf disks in sterile 0.1% Silwet L-77 in 10 mM $MgCl_2$ at 200 rpm for 1 h. *In planta Pst* was then quantified by plating a dilution series on KB medium with kanamycin (50 μg/mL) and rifampicin (100 μg/mL).

4.1.4. DHCA rescue assays

A. thaliana (7 wpg) rosette leaves (medium size, fully expanded) were inoculated with *Pst* as outlined in section 4.1.3. At 24-h post-inoculation with bacteria, DHCA (70 μg/mL (284 μM) or 250 ng/mL (1.02 μM)) was pressure-infiltrated into leaves. Mock controls consisted of 10 mM $MgCl_2$ with an equivalent amount of DMSO (the solvent used for DHCA) added. Once thoroughly dried (~1 h), plants were returned to growth chambers. Bacterial growth was quantified as outlined in section 4.1.3.

4.1.5. Intercellular washing fluid collection for metabolite profiling

Inoculations of mock- and *Pst*-solutions was completed as described in Section 4.1.3. The infiltration-centrifugation method developed by O'Leary et al. (2014) was used with some modifications for metabolite profiling. Fully expanded medium rosette leaves from mature (7 wpg) plants were detached at the petiole with a razor blade at 24 hpi with mock solution or *Pst*. Leaves were weighed to 1 g fresh weight (FW) and rinsed for 5 s in chilled, distilled water to remove surface contamination and then placed in a 60 mL syringe filled with 30 mL of chilled, distilled water. Using a gloved finger, negative pressure was created in the syringe by pulling the plunger out to the 60 mL mark and slowly releasing. This was repeated approximately three times per sample until leaves were thoroughly infiltrated (darkened transparent color throughout and negative buoyancy). Excess surface liquid was removed by blotting and the leaves were again weighed. Infiltrated leaves were stacked between layers of Parafilm and secured around a 1000 μl pipette tip placed in a cut 20 mL syringe bottom with the tip placed in a 1.5 mL microfuge tube (petioles facing upward) and centrifuged for 6 min at 600×*g* in a swinging bucket rotor at 4 °C, resulting in 150–200 μl of IWF collected per sample. After collection, leaves were visually examined to ensure IWFs were removed from all leaves (no water-soaked patches). Cytoplasmic contamination was assayed by measuring chlorophyll (664 nm) and turbidity (700 nm) as outlined in Baker et al. (2012) and IWFs were flash frozen in liquid nitrogen, stored at −80 °C, and transported to the Vineland Research and Innovation Centre under dry ice for analysis. Each of three replicates contained leaves from 13 individual plants (13 fully expanded rosette leaves).

4.1.6. Accession numbers

Sequence data for genes from this article can be found in the GenBank/EMBL data libraries under the following Arabidopsis Genome Initiative identifiers: *CYP71A12* (At2g30750), *CYP71A13* (At2g30770), *CYP71B15* (At3g26830).

4.2. Chemicals

Unless otherwise noted, all chemicals were purchased from Sigma-Aldrich (>95% purity). An initial stock of dihydrocamalexic acid for use as an UPLC-MS standard for DHCA identification was generously provided by E. Glawischnig (TUM Campus Straubing for Biotechnology and Sustainability, Technical University of Munich, Germany). Indole-3-carbonitrile and D-cysteine were purchased from Toronto Research Chemicals. UPLC-MS grade acetonitrile, water, and formic acid were purchased from Fisher Scientific.

4.3. Metabolite profiling

4.3.1. Preparation of intercellular washing fluids

100 μl aliquots of IWF were diluted in 60 μl of acetonitrile (5%) in water acidified with 0.1% formic acid. Samples were sonicated in ice water for 5 min, vortexed, sonicated for another 5 min, then centrifuged at 20,000×*g* for 2 min. The supernatant was filtered with 0.2 μm GHP filters (Acrodisc) and transferred to LC-certified vials (Waters) with 250 μl glass inserts (Chromatographic Specialties Inc). Quality control pools consisting of equal amounts of individual extracted IWFs were prepared in LC-certified vials (Waters).

4.3.2. UPLC/ESI-QTOF MS^E and MS/MS

Chromatographic separation was performed on an Acquity I-Class UPLC (Waters, Manchester, UK) equipped with an Acquity UPLC BEH C18 1.7 μm column (Waters) using a binary solvent mixture consisting of solvent A (5% acetonitrile in water with 0.1% formic acid) and solvent B (acetonitrile with 0.1% formic acid), with 5 μl (IWFs) sample injection at infusion flow rate of 0.3 mL/min. The gradient was set for solvent B at 0–40% for 0.0–22.5 min, 100% over 23.0–24.5 min, decreasing to 0% over 25.0–26.0 min (Rogachev and Aharoni, 2011). Analytic data were acquired on a Xevo G2-XS QTOF (Waters) with a capillary voltage of 3 kV (ESI+) or 2.5 kV (ESI-) and sample cone voltage of 40 eV. MS^E data were acquired in positive and negative electrospray ionization (ESI) modes and in ESI + for dihydrocamalexic acid MS/MS. A survey scan time of 0.25 s in continuum data format with an acquisition mass range of 50–1200 Da was used for MS^E with a desolvation temperature of 500 °C, cone gas flow of 50 L/h, and desolvation gas flow of 800 L/h. For MS^E, the low collision energy was 6 eV and the high ramp collision energy was 15–35 eV. MS/MS data for DHCA was acquired over 5–10 min at a mass range of 50–1200 Da and set mass of 247.05 Da [M+H] using a scan time of 0.25 s in continuum format at 25 eV collision energy. Leucine enkephelin (200 pg/μl in 50:50 acetonitrile/water with 0.1% formic acid) was used as a reference calibrant with LockSpray ion source (Waters; infusion flow rate 10 μl/min) for exact mass measurement.

4.3.3. Data acquisition

Extracts for each treatment and blanks were all injected in randomized order. Quality control samples were initially injected 10 times sequentially to equilibrate the column, then every 6 runs in both ESI+ and ESI- modes. Peak alignment, quality control assessment, peak picking, pseudomolecular ion (adduct) composition, and normalization

to all mass features was performed in Progenesis QI (Non-Linear Dynamics). Suitability of data for downstream analysis was assessed by ensuring tight clustering of quality control pooled samples in principal component analysis considering all samples. Mass features were manually processed in MassLynx 4.1 (Waters) to filter out background and identify molecular ions of interest.

4.3.4. Untargeted data analysis and compound identification

Putative metabolite identification was completed by: establishing fragmentation patterns (fragmentation in mass spectra for low and high energy (first and second function), published spectral data, adducts, neutral loss); estimating elemental composition (Range C0-100, H0-100, N0-5, O0-30, S0-3, unsaturation, 5 ppm $\geq$ *m/z* 300, 2 mDa $\leq$200); putative identification from publicly available and in-house customized natural products databases and commercially available standards where applicable. Mass error was calculated using the formula: (observed *m/z* – theoretical *m/z*)/(theoretical *m/z* * 10^6). Theoretical *m/z* were calculated in Mass Lynx 3.1. Elemental composition was calculated using ChemCalc Molecular formula based on monoisotopic mass (http://www.cheminfo.org; Patiny and Borel, 2013). Features of interest were selected by pairwise comparison (*t*-test) between wild-type (Col-0) mock- and *Pst*-inoculated IWFs, using median fold change threshold (>2) and *t*-test threshold ($P < 0.05$, two-tailed, equal variance) volcano plots. The resulting features of interest were compared across all datasets (Col-0, *cyp71a12/cyp71a13*, and *cyp71b15* mock- and *Pst*-inoculated) using normalized abundance plots and ANOVA testing ($P < 0.05$, Tukey's HSD). Two synthesized standards of dihydrocamalexic acid (2–5000 pg on column) and a commercially available standard of camalexin (1–5000 pg on column) were quantified in positive-ion mode; a commercially available standard of salicylic acid (100–5000 ng on column) was quantified in negative-ion mode. An internal standard of deuterated salicylic acid (-d_6) was added to each sample for normalization and relative quantification.

4.4. Synthesis of dihydrocamalexic acid and structural analogs

All reactions were performed in sealed glass vials or round-bottom flasks under nitrogen atmosphere. ^{1}H and ^{13}C spectra were recorded on Bruker AV 500, 600 or 700 MHz spectrometers in $CDCl_3$, DMSO-d_6, or MeOD. Bulk solvent removal was performed by rotary evaporation under reduced pressure. For reactions with solvent volumes under 3 mL, the solvent was evaporated under a stream of nitrogen. Column chromatographic purification was performed using Silicycle silica gel (40–63 μM, 230–400 mesh) with technical grade solvents. Yields are reported for spectroscopically pure compounds, unless stated otherwise. Coupling constants are recorded in Hz and chemical shifts are reported in ppm downfield of TMS. HRMS (ESI^+) was performed on a Waters Micromass Q-ToF Ultima Global. The synthesis of DHCA and derivatives is based on Maltsev et al. (2013).

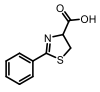

2-Phenyl-4,5-dihydrothiazole-4-carboxylic acid **1** and **2**.

Benzonitrile (103 mg, 1.00 mmol, 1.0 eq.), cysteine (181 mg, 1.50 mmol, 1.5 eq.) and sodium bicarbonate (126 mg, 1.50 mmol, 1.5 eq.) were added to a degassed solution of methanol (2.6 mL) and water (1.7 mL) in round-bottom flask under nitrogen atmosphere. Then, 50 μL of a 1 M solution of NaOH was added to the reaction mixture and the flask was sealed under nitrogen and allowed to stir overnight. MeOH was removed by rotary evaporation and the reaction mixture was washed with 2 mL of diethyl ether before being cooled to 0 °C and carefully quenched by dropwise addition of 2 M HCl until the mixture was pH 2 (indicator paper) resulting in the solution becoming cloudy. The mixture was then extracted with ethyl acetate (3 × 4 mL), the organic extracts were dried over sodium sulphate and concentrated using rotary evaporation. The crude residue was purified by filtering over a short silica column (elution with 100% ethyl acetate), followed by solvent removal. Yield = 156 mg of off-white solid (75% yield). m. p. = 110–111 °C (recrystallized from EtOAc, lit. 114–115 °C).[1] ^{1}H NMR (500 MHz, $CDCl_3$) δ 9.06 (s, 1H), 7.89–7.83 (m, 2H), 7.54–7.50 (m, 1H), 7.43 (t, *J* = 7.6 Hz, 2H), 5.38 (t, *J* = 9.3 Hz, 1H), 3.76 (dd, *J* = 10.3, 7.9 Hz, 1H), 3.72 (dd, *J* = 10.2, 8.6 Hz, 1H). ^{13}C NMR (126 MHz, $CDCl_3$) δ 173.6, 173.4, 132.5, 132.0, 128.8, 128.8, 77.8, 35.1. For (*R*)-2-Phenyl-4,5-dihydrothiazole-4-carboxylic acid (derived from L-cysteine) **1**, [alpha]D25 = +37.1 (c 0.36, MeOH). For (*S*)-2-phenyl-4,5-dihydrothiazole-4-carboxylic acid **2** (derived from D-cysteine), [alpha]D21 = −34.9 (c 0.37, MeOH). ESI HRMS expected for $C_{10}H_{10}NO_2S$ $(M + H)^+$: 208.0427 found 208.0404.

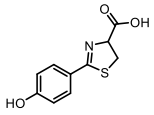

2-(4-hydroxyphenyl)-4,5-dihydrothiazole-4-carboxylic acid (monohydrate) **3** and **4**.

4-cyanophenol (119 mg, 1.00 mmol, 1.0 eq.), cysteine (242 mg, 2.00 mmol, 2.0 eq.), and sodium bicarbonate (336 mg, 4.00 mmol, 4.0 eq.) were added to 4 mL of degassed absolute ethanol in a pressure vial. The vial was sealed under nitrogen and heated with stirring in a 100 °C oil bath for 24 h. The reaction was removed from the oil bath and cooled to room temperature and the ethanol was removed using rotary evaporation. The residue was washed with 2 mL of ethyl acetate, suspended in 2 mL of water, cooled to 0 °C and carefully quenched by dropwise addition of 2 M HCl until the mixture was pH 2 (indicator paper). The resulting mixture was extracted with ethyl acetate (3 × 4 mL) and the combined organic extracts were dried over sodium sulphate before concentration using rotary evaporation. The resulting solid was washed with 0.5 mL of water to remove trace salts and dried leaving the desired product. Yield = 178 mg (80% yield) of a white powder. m. p. = 151–153 (decomposition; powder recovered from MeOH; lit. 151–153 °C).[1] ^{1}H NMR (500 MHz, DMSO) δ 12.92 (s, 1H), 10.15 (s, 1H), 7.63 (d, *J* = 8.7 Hz, 2H), 6.84 (d, *J* = 8.7 Hz, 2H), 5.21 (dd, *J* = 9.3, 8.1 Hz, 1H), 3.65 (dd, *J* = 11.1, 9.3 Hz, 1H), 3.55 (dd, *J* = 11.1, 8.1 Hz, 1H). ^{13}C NMR (126 MHz, DMSO) δ 172.1, 167.7, 160.7, 130.1, 123.4, 115.5, 78.1, 34.8. For (*R*)-2-(4-hydroxyphenyl)-4,5-dihydrothiazole-4-carboxylic acid **3** (derived from L-cysteine), [alpha]D25 = −12.4 (c 0.1, MeOH). For (*S*)-2-(4-hydroxyphenyl)-4,5-dihydrothiazole-4-carboxylic acid **4** (derived from D-cysteine), [alpha]D25 = +12.3 (c 0.1, MeOH). ESI HRMS expected for $C_{10}H_8NO_3S$ $(M\text{-}H)^-$: 222.0230 found 222.0236.

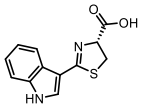

(*R*)-2-(3-Indolyl)-4,5-dihydrothiazole-4-carboxylic acid (DHCA):

3-cyanoindole (36 mg, 0.25 mmol, 1.0 eq.), L-cysteine (60 mg, 0.50 mmol, 2.0 eq.) and sodium bicarbonate (84 mg, 1.00 mmol, 4.0 eq.) were added to 1 mL of degassed ethanol in a microwave vial. The vial was sealed under nitrogen and heated with stirring in a 100 °C oil bath for 36 h. The reaction was removed from the oil bath and cooled to room temperature and the ethanol was removed using rotary evaporation. The residue was washed with 1 mL of ethyl acetate, suspended in 0.5 mL of water, cooled to 0 °C and carefully quenched by dropwise addition of 2 M HCl until the mixture was pH 2 (indicator paper), resulting in the precipitation of a small amount of tan solid. The solution was stored in a refrigerator overnight and the solid was filtered and washed with 2 mL of water, leaving the desired product. Yield = 26 mg of a tan powder (42% yield). m. p. = 145–148 °C (decomposition; powder precipitated

from H_2O). ^1H NMR (600 MHz, MeOD) δ 8.36 (s, 1H), 8.05–7.99 (m, 1H), 7.58–7.53 (m, 1H), 7.37–7.30 (m, 2H), 5.29–5.24 (m, 1H), 4.05–3.93 (m, 2H). ^{13}C NMR (151 MHz, MeOD) δ 177.1, 172.6, 138.8, 135.9, 126.0, 125.4, 124.4, 121.1, 114.2, 107.1, 69.2, 35.6. [alpha]D25 = −62.9 (c 0.2, MeOH). ESI HRMS expected for $C_{12}H_{11}N_2O_2S$ $(M + H)^+$: 247.0536 found 247.0532.

4.5. Antimicrobial activity assessment

4.5.1. Planktonic bacterial growth assays

Minimum inhibitory concentration (MIC) and minimum bactericidal concentration (MBC) of tested indolic compounds and salicylic acid were determined using the micro-dilution broth method (Wiegand et al., 2008). *Pst* overnight cultures (OD_{600} = 0.2 to 0.6) were prepared for growth assays as outlined in Wilson et al. (2017) in *Hrp*-inducing minimal (HIM) liquid medium (Huynh et al., 1989). Serial dilutions of compounds were prepared in ethanol (SA, camalexin) or DMSO (SA, DHCA, and DHCA analogs). A series of two-fold dilutions of DHCA, SA camalexin, or DHCA analogs were prepared ranging from 0.05 to 1 mg/mL in HIM medium in sterile non-tissue-culture-treated 96-well microtiter plates (Corning Life Sciences). Bacterial inoculum was added to each well to obtain a final optical density value of OD_{600} = 0.05. Solvent (DMSO or ethanol) and sterile (media only) controls were included. Plates were incubated at room temperature (24–26 °C) in a plate reader with shaking (Tecan Sunrise). Optical density (OD_{600}) was measured every 15 min for 68 or 72 h. The MIC was assessed visually as the lowest concentration of compound showing total bacterial growth inhibition during the mid-exponential growth phase of controls (~36 h) without killing bacteria. The MBC of each compound was determined as the lowest concentration to kill bacteria, as defined by sub-cultures from pooled wells exhibiting no bacterial growth on KB media plates without antibiotics to prevent additive interactions between compounds creating false MBC results (Balouiri et al., 2016). Each experiment was performed at least twice, and representative data are presented.

4.5.2. Dihydrocamalexic acid bacterial metabolism assays

To test for *Pst*'s ability to utilize dihydrocamalexic acid (DHCA) as a carbon source or as a nitrogen and sulfur source, bacteria were grown in *Hrp*-inducing minimal medium with DHCA as outlined in section 4.6.1 with the following alterations. To test the ability of *Pst* to use DHCA as a carbon source, bacteria were incubated with DHCA in HIM medium without a carbon source (lacking fructose). To test for ability of *Pst* to use DHCA as a nitrogen and/or sulfur source, bacteria were incubated with DHCA in HIM medium without a nitrogen and sulfur source (lacking ammonium sulphate).

4.5.3. In vitro biofilm assays

Biofilm formation of surface-adherent *Pst* cells was quantified using the method developed by O'Toole (2011). Cultures, compounds, and microtiter plates were prepared as outlined in section 4.6.1. Plates were incubated without shaking in darkness at room temperature (24–26 °C). At 24, 36, 48, 60 and 72 h, plates were rinsed thoroughly in water to remove planktonic bacteria, incubated with 0.1% crystal violet for 10 min to stain biofilm, rinsed to remove extra strain and any planktonic bacteria remaining, and left overnight to dry. To de-stain for biofilm quantification, plates were incubated with 30% acetic acid (200 µl per well) for 15 min. Optical density (OD_{570}) was recorded on a plate reader (Biotek Synergy 2). Each experiment was repeated twice, and representative data are presented.

4.6. Statistical analyses and software

Mass feature normalized relative abundance was completed in Progenesis QI (Nonlinear Dynamics). Principal component analysis, volcano plots (raw $P < 0.05$, fold-change > 2), Brown-Forsythe, and one-way analysis of variance (ANOVA; $P < 0.05$, Tukey's HSD or Dunnett's MCT) statistical analyses were performed in Metaboanalyst 3.1 (www.metaboanalyst.ca; Xia and Wishart, 2016), R, and Prism 9.0 (GraphPad). One-way ANOVA was used to determine statistically significant differences in bacterial levels *in planta* with normality and homogeneity of variance assessed by the Sharpio-Wilk test and Levene's test. Means with unequal variances were log-transformed before analysis. Tukey's HSD post hoc test was used for comparisons ($p < 0.05$) among mutants and wild-type plants. All non-metabolomic statistical tests were completed in R and Prism 6.0 and 7.0 (GraphPad). Molecules were drawn in ChemDraw (PerkinElmer).

Declaration of competing interest

The authors declare that they have no known competing financial interests or personal relationships that could have appeared to influence the work reported in this paper.

Acknowledgements

We are especially grateful to Erich Glawischnig (TUM Campus Straubing for Biotechnology and Sustainability, Technical University of Munich, Germany) for providing the *cyp71a12/a13-1* double mutant seed and a synthesized standard of dihydrocamalexic acid to confirm our metabolite identification. Thank you to Jane Glazebrook (University of Minnesota, St. Paul, MN, USA) for providing *cyp71b15* (*pad3-1*) mutant seed, E. Weretilnyk (McMaster University, Dept. Of Biology) for providing thermocycler access, and J. Wilson (McMaster University, Dept. Of Biology) for providing access to the Biotek Synergy 2 plate reader for biofilm assays. *In vitro* antibacterial assays were performed at the McMaster Centre for Microbial Chemical Biology. This work has been supported by Growing Forward 2 and Canada Foundation for Innovation funding awarded to Vineland Research and Innovation Centre, an Ontario Graduate Scholarship to C. Kempthorne, an NSERC Discovery Grant to J. McNulty, NSERC Scholarships to A. Nielsen and D. Wilson, and an NSERC Discovery and Research Infrastructure grant to R. Cameron.

Appendix A. Supplementary data

Supplementary data to this article can be found online at https://doi.org/10.1016/j.phytochem.2021.112747.

References

Agrawal, G.K., Jwa, N.-S., Lebrun, M.-H., Job, D., Rakwal, R., 2010. Plant secretome: unlocking secrets of the secreted proteins. Proteomics 10, 799–827. https://doi.org/10.1002/pmic.200900514.

Baccelli, I., Lombardi, L., Luti, S., Bernardi, R., Picciarelli, P., Scala, A., Pazzagli, L., 2014. Cerato-platanin induces resistance in arabidopsis leaves through stomatal perception, overexpression of salicylic acid- and ethylene-signalling genes and camalexin biosynthesis. PloS One 9, e100959. https://doi.org/10.1371/journal.pone.0100959.

Baker, C.J., Kovalskaya, N.Y., Mock, N.M., Owens, R.A., Deahl, K.L., Whitaker, B.D., Roberts, D.P., Hammond, R.W., Aver'yanov, A.A., 2012. An internal standard technique for improved quantitative analysis of apoplastic metabolites in tomato leaves. Physiol. Mol. Plant Pathol. 78, 31–37. https://doi.org/10.1016/j.pmpp.2012.01.001.

Balouiri, M., Sadiki, M., Ibnsouda, S.K., 2016. Methods for in vitro evaluating antimicrobial activity: A review. J. Pharmaceut. Anal. 6 (2) https://doi.org/10.1016/j.jpha.2015.11.005.

Bednarek, P., Osbourn, A., 2009. Plant-microbe interactions: chemical diversity in plant defense. Science 324, 746–748. https://doi.org/10.1126/science.1171661.

Bednarek, P., Schneider, B., Svatoš, A., Oldham, N.J., Hahlbrock, K., 2005. Structural complexity, differential response to infection, and tissue specificity of indolic and phenylpropanoid secondary metabolism in arabidopsis roots. Plant Physiol. 138, 1058–1070. https://doi.org/10.1104/pp.104.057794.

Böttcher, C., Chapman, A., Fellermeier, F., Choudhary, M., Scheel, D., Glawischnig, E., 2014. The biosynthetic pathway of indole-3-carbaldehyde and indole-3-carboxylic acid derivatives in arabidopsis. Plant Physiol. 165, 841–853. https://doi.org/10.1104/pp.114.235630.

Böttcher, C., Westphal, L., Schmotz, C., Prade, E., Scheel, D., Glawischnig, E., 2009. The multifunctional enzyme CYP71B15 (PHYTOALEXIN DEFICIENT3) converts cysteine-

indole-3-acetonitrile to camalexin in the indole-3-acetonitrile metabolic network of Arabidopsis thaliana. Plant Cell 21, 1830–1845. https://doi.org/10.1105/tpc.109.066670.
Cameron, R.K., Zaton, K., 2004. Intercellular salicylic acid accumulation is important for age-related resistance in Arabidopsis to Pseudomonas syringae. Physiol. Mol. Plant Pathol. 65, 197–209. https://doi.org/10.1016/j.pmpp.2005.02.002.
Carviel, J.L., Wilson, D.C., Isaacs, M., Carella, P., Catana, V., Golding, B., Weretilnyk, E. A., Cameron, R.K., 2014. Investigation of intercellular salicylic acid accumulation during compatible and incompatible arabidopsis-Pseudomonas syringae interactions using a fast neutron-generated mutant allele of EDS5 identified by genetic mapping and whole-genome sequencing. PloS One 9, e88608. https://doi.org/10.1371/journal.pone.0088608.
Costerton, J.W., Stewart, P.S., Greenberg, E.P., 1999. Bacterial biofilms: a common cause of persistent infections. Science 284, 1318–1322. https://doi.org/10.1126/science.284.5418.1318.
Darvill, A.G., Albersheim, P., 1984. Phytoalexins and their elicitors-a defense against microbial infection in plants. Annu. Rev. Plant Physiol. 35 (1), 243–275.
de Kievit, T., Seed, P.C., Nezezon, J., Passador, L., Iglewski, B.H., 1999. RsaL, a novel repressor of virulence gene expression in Pseudomonas aeruginosa. J. Bacteriol. 181, 2175–2184. https://doi.org/10.1128/JB.181.7.2175-2184.1999.
Delaunois, B., Jeandet, P., ClÃ©ment, C., Baillieul, F., Dorey, S., Cordelier, S., 2014. Uncovering plant-pathogen crosstalk through apoplastic proteomic studies. Front. Plant Sci. 5 https://doi.org/10.3389/fpls.2014.00249.
DeRidder, B.P., Goldsbrough, P.B., 2006. Organ-specific expression of glutathione S -transferases and the efficacy of herbicide safeners in arabidopsis. Plant Physiol. 140, 167–175. https://doi.org/10.1104/pp.105.067199.
Destro, T., Prasad, D., Martignago, D., Lliso Bernet, I., Trentin, A.R., Renu, I.K., Ferretti, M., Masi, A., 2011. Compensatory expression and substrate inducibility of -glutamyl transferase GGT2 isoform in Arabidopsis thaliana. J. Exp. Bot. 62, 805–814. https://doi.org/10.1093/jxb/erq316.
Develey-Rivière, M.-P., Galiana, E., 2007. Resistance to pathogens and host developmental stage: a multifaceted relationship within the plant kingdom. New Phytol. 175, 405–416. https://doi.org/10.1111/j.1469-8137.2007.02130.x.
Donlan, R.M., Costerton, J.W., 2002. Biofilms: survival mechanisms of clinically relevant microorganisms. Clin. Microbiol. Rev. 15, 167–193. https://doi.org/10.1128/CMR.15.2.167-193.2002.
Forcat, S., Bennett, M., Grant, M., Mansfield, J.W., 2010. Rapid linkage of indole carboxylic acid to the plant cell wall identified as a component of basal defence in Arabidopsis against hrp mutant bacteria. Phytochemistry 71, 870–876. https://doi.org/10.1016/j.phytochem.2010.03.010.
Frerigmann, H., Glawischnig, E., Gigolashvili, T., 2015. The role of MYB34, MYB51 and MYB122 in the regulation of camalexin biosynthesis in Arabidopsis thaliana. Front. Plant Sci. 6 https://doi.org/10.3389/fpls.2015.00654.
Gentzel, I., Giese, L., Zhao, W., Alonso, A.P., Mackey, D., 2019. A simple method for measuring apoplast hydration and collecting apoplast contents. Plant Physiol. 179, 1265–1272. https://doi.org/10.1104/pp.18.01076.
Geu-Flores, F., Møldrup, M.E., Böttcher, C., Olsen, C.E., Scheel, D., Halkier, B.A., 2011. Cytosolic γ-glutamyl peptidases process glutathione conjugates in the biosynthesis of glucosinolates and camalexin in arabidopsis. Plant Cell 23, 2456–2469. https://doi.org/10.1105/tpc.111.083998.
Ghods, S., Sims, I.M., Moradali, M.F., Rehm, B.H.A., 2015. Bactericidal compounds controlling growth of the plant pathogen Pseudomonas syringae pv. actinidiae, which forms biofilms composed of a novel exopolysaccharide. Appl. Environ. Microbiol. 81, 4026–4036. https://doi.org/10.1128/AEM.00194-15.
Glawischnig, E., Hansen, B.G., Olsen, C.E., Halkier, B.A., 2004. Camalexin is synthesized from indole-3-acetaldoxime, a key branching point between primary and secondary metabolism in Arabidopsis. Proc. Natl. Acad. Sci. Unit. States Am. 101, 8245–8250. https://doi.org/10.1073/pnas.0305876101.
Glazebrook, J., Ausubel, F.M., 1994. Isolation of phytoalexin-deficient mutants of Arabidopsis thaliana and characterization of their interactions with bacterial pathogens. Proc. Natl. Acad. Sci. Unit. States Am. 91, 8955–8959. https://doi.org/10.1073/pnas.91.19.8955.
Hagemeier, J., Schneider, B., Oldham, N.J., Hahlbrock, K., 2001. Accumulation of soluble and wall-bound indolic metabolites in Arabidopsis thaliana leaves infected with virulent or avirulent Pseudomonas syringae pathovar tomato strains. Proc. Natl. Acad. Sci. Unit. States Am. 98, 753–758. https://doi.org/10.1073/pnas.98.2.753.
Hutt, A.G., O'Grady, J., 1996. Drug chirality: a consideration of the significance of the stereochemistry of antimicrobial agents. J. Antimicrob. Chemother. 37, 7–32. https://doi.org/10.1093/jac/37.1.7.
Huynh, T., Dahlbeck, D., Staskawicz, B., 1989. Bacterial blight of soybean: regulation of a pathogen gene determining host cultivar specificity. Science 245, 1374–1377. https://doi.org/10.1126/science.2781284.
Iven, T., König, S., Singh, S., Braus-Stromeyer, S.A., Bischoff, M., Tietze, L.F., Braus, G.H., Lipka, V., Feussner, I., Dröge-Laser, W., 2012. Transcriptional activation and production of tryptophan-derived secondary metabolites in arabidopsis roots contributes to the defense against the fungal vascular pathogen verticillium longisporum. Mol. Plant 5, 1389–1402. https://doi.org/10.1093/mp/sss044.
Kariñho-Betancourt, E., Agrawal, A.A., Halitschke, R., Núñez-Farfán, J., 2015. Phylogenetic correlations among chemical and physical plant defenses change with ontogeny. New Phytol. 206, 796–806. https://doi.org/10.1111/nph.13300.
Khameneh, B., Iranshahy, M., Soheili, V., Fazly Bazzaz, B.S., 2019. Review on plant antimicrobials: a mechanistic viewpoint. Antimicrob. Resist. Infect. Contr. 8, 118. https://doi.org/10.1186/s13756-019-0559-6.
Kim, B.J., Park, J.H., Park, T.H., Bronstein, P.A., Schneider, D.J., Cartinhour, S.W., Shuler, M.L., 2009. Effect of iron concentration on the growth rate of Pseudomonas syringae and the expression of virulence factors in hrp-inducing minimal medium. Appl. Environ. Microbiol. 75, 2720–2726. https://doi.org/10.1128/AEM.02738-08.
Klein, A.P., Anarat-Cappillino, G., Sattely, E.S., 2013. Minimum set of cytochromes P450 for reconstituting the biosynthesis of camalexin, a major arabidopsis antibiotic. Angew. Chem. 125, 13870–13873. https://doi.org/10.1002/ange.201307454.
Kus, J.V., Zaton, K., Sarkar, R., Cameron, R.K., 2002. Age-related resistance in arabidopsis is a developmentally regulated defense response to Pseudomonas syringae. Plant Cell 14, 479–490. https://doi.org/10.1105/tpc.010481.
Lee, J.-H., Kim, Y.-G., Kim, C.-J., Lee, J.-C., Cho, M.H., Lee, J., 2012. Indole-3-acetaldehyde from Rhodococcus sp. BFI 332 inhibits Escherichia coli O157:H7 biofilm formation. Appl. Microbiol. Biotechnol. 96, 1071–1078. https://doi.org/10.1007/s00253-012-3881-y.
Lewis, K., Ausubel, F.M., 2006. Prospects for plant-derived antibacterials. Nat. Biotechnol. 24, 1504–1507. https://doi.org/10.1038/nbt1206-1504.
Lu, Y.-P., Li, Z.-S., Rea, P.A., 1997. AtMRP1 gene of Arabidopsis encodes a glutathione S-conjugate pump: isolation and functional definition of a plant ATP-binding cassette transporter gene. Proc. Natl. Acad. Sci. Unit. States Am. 94, 8243–8248. https://doi.org/10.1073/pnas.94.15.8243.
Maltsev, O., Walter, V., Brandl, M., Hintermann, L., 2013. Medium buffer effects on the condensation of l-cysteine and aryl nitriles to (R)-2-Aryl-4,5-dihydrothiazole-4-carboxylic acids. Synthesis 45, 2763–2767. https://doi.org/10.1055/s-0033-1339492.
Manoharan, B., Neale, H.C., Hancock, J.T., Jackson, R.W., Arnold, D.L., 2015. The identification of genes important in Pseudomonas syringae pv. phaseolicola plant colonisation using in vitro screening of transposon libraries. PloS One 10, e0137355. https://doi.org/10.1371/journal.pone.0137355.
Mansfeld, B.N., Colle, M., Kang, Y., Jones, A.D., Grumet, R., 2017. Transcriptomic and metabolomic analyses of cucumber fruit peels reveal a developmental increase in terpenoid glycosides associated with age-related resistance to Phytophthora capsici. Hortic. Res. 4, 17022. https://doi.org/10.1038/hortres.2017.22.
Martin, M.N., Saladores, P.H., Lambert, E., Hudson, A.O., Leustek, T., 2007. Localization of members of the γ -glutamyl transpeptidase family identifies sites of glutathione and glutathione S -conjugate hydrolysis. Plant Physiol. 144, 1715–1732. https://doi.org/10.1104/pp.106.094409.
Masák, J., Čejková, A., Schreiberová, O., Řezanka, T., 2014. Pseudomonas biofilms: possibilities of their control. FEMS Microbiol. Ecol. 89, 1–14. https://doi.org/10.1111/1574-6941.12344.
Melotto, M., Underwood, W., Koczan, J., Nomura, K., He, S.Y., 2006. Plant stomata function in innate immunity against bacterial invasion. Cell 126, 969–980. https://doi.org/10.1016/j.cell.2006.06.054.
Møldrup, M.E., Salomonsen, B., Geu-Flores, F., Olsen, C.E., Halkier, B.A., 2013a. De novo genetic engineering of the camalexin biosynthetic pathway. J. Biotechnol. 167, 296–301. https://doi.org/10.1016/j.jbiotec.2013.06.013.
Møldrup, M.E., Geu-Flores, F., Halkier, B.A., 2013b. Assigning gene function in biosynthetic pathways: camalexin and beyond. Plant Cell 25, 360–367. https://doi.org/10.1105/tpc.112.104745.
Mucha, S., Heinzlmeir, S., Kriechbaumer, V., Strickland, B., Kirchhelle, C., Choudhary, M., Kowalski, N., Eichmann, R., Hückelhoven, R., Grill, E., Kuster, B., 2019. The formation of a camalexin biosynthetic metabolon. Plant Cell 31 (11), 2697–2710. https://doi.org/10.1105/tpc.19.00403.
Müller, T.M., Böttcher, C., Glawischnig, E., 2019. Dissection of the network of indolic defence compounds in Arabidopsis thaliana by multiple mutant analysis. Phytochemistry 161, 11–20. https://doi.org/10.1016/j.phytochem.2019.01.009.
Müller, T.M., Böttcher, C., Morbitzer, R., Götz, C.C., Lehmann, J., Lahaye, T., Glawischnig, E., 2015. TRANSCRIPTION ACTIVATOR-LIKE EFFECTOR NUCLEASE-mediated generation and metabolic analysis of camalexin-deficient cyp71a12 cyp71a13 double knockout lines. Plant Physiol. 168, 849–858. https://doi.org/10.1104/pp.15.00481.
Murashige, T., Skoog, F., 1962. A revised medium for rapid growth and bio assays with tobacco tissue cultures. Physiol. Plantarum 15 (3), 473–497.
Nafisi, M., Goregaoker, S., Botanga, C.J., Glawischnig, E., Olsen, C.E., Halkier, B.A., Glazebrook, J., 2007. Arabidopsis cytochrome P450 monooxygenase 71A13 catalyzes the conversion of indole-3-acetaldoxime in camalexin synthesis. Plant Cell 19, 2039–2052. https://doi.org/10.1105/tpc.107.051383.
Nafisi, M., Sønderby, I.E., Hansen, B.G., Geu-Flores, F., Nour-Eldin, H.H., Nørholm, M.H. H., Jensen, N.B., Li, J., Halkier, B.A., 2006. Cytochromes P450 in the biosynthesis of glucosinolates and indole alkaloids. Phytochemistry Rev. 5, 331–346. https://doi.org/10.1007/s11101-006-9004-6.
Naseem, M., Kunz, M., Dandekar, T., 2017. Plant–pathogen maneuvering over apoplastic sugars. Trends Plant Sci. 22, 740–743. https://doi.org/10.1016/j.tplants.2017.07.001.
O'Leary, B.M., Neale, H.C., Geilfus, C.-M., Jackson, R.W., Arnold, D.L., Preston, G.M., 2016. Early changes in apoplast composition associated with defence and disease in interactions between Phaseolus vulgaris and the halo blight pathogen Pseudomonas syringae Pv. phaseolicola. Plant. Cell Environ. 39, 2172–2184. https://doi.org/10.1111/pce.12770.
O'Leary, B.M., Rico, A., McCraw, S., Fones, H.N., Preston, G.M., 2014. The infiltration-centrifugation technique for extraction of apoplastic fluid from plant leaves using Phaseolus vulgaris as an example. JoVE. https://doi.org/10.3791/52113.
O'Toole, G.A., 2011. Microtiter dish biofilm formation assay. JoVE. https://doi.org/10.3791/2437.
Ohkama-Ohtsu, N., Radwan, S., Peterson, A., Zhao, P., Badr, A.F., Xiang, C., Oliver, D.J., 2007. Characterization of the extracellular γ-glutamyl transpeptidases, GGT1 and GGT2, in Arabidopsis. Plant J. 49, 865–877. https://doi.org/10.1111/j.1365-313X.2006.03004.x.

Pastorczyk, M., Kosaka, A., Piślewska-Bednarek, M., López, G., Frerigmann, H., Kułak, K., Glawischnig, E., Molina, A., Takano, Y., Bednarek, P., 2020. The role of <scp>CYP</scp> 71A12 monooxygenase in pathogen-triggered tryptophan metabolism and Arabidopsis immunity. New Phytol. 225, 400–412. https://doi.org/10.1111/nph.16118.

Patiny, L., Borel, A., 2013. ChemCalc: A building block for tomorrow's chemical infrastructure. J. Chem. Inf. Model. 53 (5), 1223–1228. https://doi.org/10.1021/ci300563h.

Pedras, M.S.C., Abdoli, A., 2017. Pathogen inactivation of cruciferous phytoalexins: detoxification reactions, enzymes and inhibitors. RSC Adv. 7, 23633–23646. https://doi.org/10.1039/C7RA01574G.

Pedras, M.S.C., Minic, Z., Abdoli, A., 2014. The phytoalexin camalexin induces fundamental changes in the proteome of Alternaria brassicicola different from those caused by brassinin. Fungal Biol 118, 83–93. https://doi.org/10.1016/j.funbio.2013.11.005.

Pedras, M.S.C., Yaya, E.E., Glawischnig, E., 2011. The phytoalexins from cultivated and wild crucifers: Chemistry and biology. Nat. Prod. Rep. 28, 1381. https://doi.org/10.1039/c1np00020a.

Rahme, L.G., Mindrinos, M.N., Panopoulos, N.J., 1992. Plant and environmental sensory signals control the expression of hrp genes in Pseudomonas syringae pv. phaseolicola. J. Bacteriol. 174, 3499–3507. https://doi.org/10.1128/JB.174.11.3499-3507.1992.

Rajniak, J., Barco, B., Clay, N.K., Sattely, E.S., 2015. A new cyanogenic metabolite in Arabidopsis required for inducible pathogen defence. Nature 525, 376–379. https://doi.org/10.1038/nature14907.

Rogachev, I., Aharoni, A., 2011. UPLC-MS-Based Metabolite Analysis in Tomato, pp. 129–144. https://doi.org/10.1007/978-1-61779-594-7_9.

Rogers, E.E., Glazebrook, J., Ausubel, F.M., 1996. Mode of action of the Arabidopsis thaliana phytoalexin camalexin and its role in Arabidopsis-pathogen interactions. Mol. Plant Microbe Interact. 9, 748–757. https://doi.org/10.1094/mpmi-9-0748.

Rusterucci, C., Zhao, Z., Haines, K., Mellersh, D., Neumann, M., Cameron, R.K., 2005. Age-related resistance to Pseudomonas syringae pv. tomato is associated with the transition to flowering in Arabidopsis and is effective against Peronospora parasitica. Physiol. Mol. Plant Pathol. 66, 222–231. https://doi.org/10.1016/j.pmpp.2005.08.004.

Schuhegger, R., Nafisi, M., Mansourova, M., Petersen, B.L., Olsen, C.E., Svatoš, A., Halkier, B.A., Glawischnig, E., 2006. CYP71B15 (PAD3) catalyzes the final step in camalexin biosynthesis. Plant Physiol. 141, 1248–1254. https://doi.org/10.1104/pp.106.082024.

Silva, L.N., Zimmer, K.R., Macedo, A.J., Trentin, D.S., 2016. Plant natural products targeting bacterial virulence factors. Chem. Rev. 116, 9162–9236. https://doi.org/10.1021/acs.chemrev.6b00184.

Smith, S.W., 2009. Chiral toxicology: it's the same Thing…Only different. Toxicol. Sci. 110, 4–30. https://doi.org/10.1093/toxsci/kfp097.

Soylu, S., Brown, I., Mansfield, J.W., 2005. Cellular reactions in Arabidopsis following challenge by strains of Pseudomonas syringae: from basal resistance to compatibility. Physiol. Mol. Plant Pathol. 66, 232–243. https://doi.org/10.1016/j.pmpp.2005.08.005.

Su, T., Xu, J., Li, Y., Lei, L., Zhao, L., Yang, H., Feng, J., Liu, G., Ren, D., 2011. Glutathione-Indole-3-Acetonitrile is required for camalexin biosynthesis in Arabidopsis thaliana. Plant Cell 23, 364–380. https://doi.org/10.1105/tpc.110.079145.

Tan, J., Bednarek, P., Liu, J., Schneider, B., Svatoš, A., Hahlbrock, K., 2004. Universally occurring phenylpropanoid and species-specific indolic metabolites in infected and uninfected Arabidopsis thaliana roots and leaves. Phytochemistry 65, 691–699. https://doi.org/10.1016/j.phytochem.2003.12.009.

Tommasini, R., Vogt, E., Fromenteau, M., Hörtensteiner, S., Matile, P., Amrhein, N., Martinoia, E., 1998. An ABC-transporter of Arabidopsis thaliana has both glutathione-conjugate and chlorophyll catabolite transport activity. Plant J. 13, 773–780. https://doi.org/10.1046/j.1365-313X.1998.00076.x.

Tucker, C., Avila-Sakar, G., 2010. Ontogenetic changes in tolerance to herbivory in Arabidopsis. Oecologia 164, 1005–1015. https://doi.org/10.1007/s00442-010-1738-6.

Whalen, M.C., 2005. Host defence in a developmental context. Mol. Plant Pathol. 6, 347–360. https://doi.org/10.1111/j.1364-3703.2005.00286.x.

Whalen, M.C., Innes, R.W., Bent, A.F., Staskawicz, B.J., 1991. Identification of Pseudomonas syringae pathogens of Arabidopsis and a bacterial locus determining avirulence on both Arabidopsis and soybean. Plant Cell 3 (1), 49–59. https://doi.org/10.1105/tpc.3.1.49.

Wiegand, I., Hilpert, K., Hancock, R., 2008. Agar and broth dilution methods to determine the minimal inhibitory concentration (MIC) of antimicrobial substances. Nat. Prot. 3, 163–175. https://doi.org/10.1038/nprot.2007.521.

Wilson, D.C., Kempthorne, C.J., Carella, P., Liscombe, D.K., Cameron, R.K., 2017. Age-related resistance in Arabidopsis thaliana involves the MADS-domain transcription factor SHORT VEGETATIVE PHASE and direct action of salicylic acid on Pseudomonas syringae. Mol. Plant Microbe Interact. 30, 919–929. https://doi.org/10.1094/MPMI-07-17-0172-R.

Xia, J., Wishart, D.S., 2016. Using MetaboAnalyst 3.0 for comprehensive metabolomics data analysis. Curr. Protoc. Bioinforma. 55 https://doi.org/10.1002/cpbi.11.

Zandalinas, S.I., Vives-Peris, V., Gómez-Cadenas, A., Arbona, V., 2012. A fast and precise method to identify indolic glucosinolates and camalexin in plants by combining mass spectrometric and biological information. J. Agric. Food Chem. 60, 8648–8658. https://doi.org/10.1021/jf302482y.

Zhao, Y., 2002. Trp-dependent auxin biosynthesis in Arabidopsis: involvement of cytochrome P450s CYP79B2 and CYP79B3. Genes Dev. 16, 3100–3112. https://doi.org/10.1101/gad.1035402.

Zhou, N., Tootle, T.L., Glazebrook, J., 1999. Arabidopsis PAD3 , a gene required for camalexin biosynthesis, encodes a putative cytochrome P450 monooxygenase. Plant Cell 11, 2419–2428. https://doi.org/10.1105/tpc.11.12.2419.